Physics Guide to CEPXS: A Multigroup Coupled Electron-Photon Cross-Section Generating Code

Version 1.0

L. J. Lorence, Jr., J. E. Morel, G. D. Valdez

SF2900Q(8-81)

PHYSICS GUIDE TO CEPXS:
A MULTIGROUP COUPLED ELECTRON-PHOTON
CROSS-SECTION GENERATING CODE
Version 1.0

L. J. Lorence, Jr.
Simulation Physics Division, 1231
Sandia National Laboratories
Albuquerque, NM 87185

J. E. Morel
Los Alamos National Laboratory
Los Alamos, NM 87545

G. D. Valdez
Applied Methods Inc.
428 Louisiana SE
Albuquerque, NM 87108

ABSTRACT

CEPXS is a multigroup-Legendre cross-section generating code. The multigroup-Legendre cross sections produced by CEPXS enable coupled electron-photon transport calculations to be performed with the one-dimensional discrete ordinates code, ONEDANT. We recommend that the 1989 version of ONEDANT that contains linear-discontinuous spatial differencing and S2 synthetic acceleration be used for such calculations. CEPXS/ONEDANT effectively solves the Boltzmann-CSD transport equation for electrons and the Boltzmann transport equation for photons over the energy range from 100 MeV to 1.0 keV. The continuous slowing-down approximation is used for those electron interactions that result in small-energy losses. The extended transport correction is applied to the forward-peaked elastic scattering cross section for electrons. A standard multigroup-Legendre treatment is used for the other coupled electron-photon cross sections. CEPXS extracts electron cross-section information from the DATAPAC data set and photon cross-section information from Biggs-Lighthill data. The model that is used for ionization/relaxation in CEPXS is essentially the same as that employed in ITS.

ACKNOWLEDGEMENTS

TABLE OF CONTENTS

I. CROSS SECTIONS

I.1 INTRODUCTION

A macroscopic cross section, $\sigma(r,E)$, can be defined as the probability that a particle undergoes an interaction per unit pathlength of travel. Such cross sections have units of inverse length and depend on the kinetic energy, E, of the particle and its spatial position, r.

Other macroscopic cross sections define the probability that particles emerge from an interaction with specified energies and angles. These differential macroscopic cross sections also depend on the energy, E', of the emergent particle and Ω'', the difference between the directions of the emergent particle and of the incident particle:

$$\sigma(r,E \rightarrow E',\Omega'') = \frac{d\sigma(r,E,E',\Omega'')}{dE' d\Omega''} \tag{I.1}$$

Differential macroscopic cross sections have units of inverse length per energy per steradian.

Since differential cross sections do not depend on the azimuthal component of Ω'', these cross sections may be expressed as:

$$\sigma(r,E \rightarrow E',\mu) = \frac{1}{2\pi} \frac{d\sigma(r,E,E',\mu)}{dE' d\mu} \tag{I.2}$$

In CEPXS, it is assumed that the differential cross sections are also separable in energy and angle:

$$\sigma(r,E \rightarrow E',\mu) = \frac{1}{2\pi} \frac{d\sigma(r,E,E')}{dE'} \frac{df(\mu)}{d\mu} \tag{I.3}$$

where $f(\mu)$ is a normalized angular distribution.

The energy and angular variations of coupled electron-photon cross sections can be represented by multigroup-Legendre expansions. The coefficients of these expansions are called multigroup-Legendre "cross sections" [BELL]. Standard discrete ordinates codes use cross section data in this form. Neutron-gamma transport calculations are commonly performed with discrete ordinates codes. However, a production discrete ordinates code for electron-photon transport calculations has not heretofore been available. The cross sections produced by CEPXS permit such calculations to be performed with the standard discrete ordinates code, ONEDANT.

The only standard discrete ordinates code that we recommend for use in

conjunction with CEPXS is the 1989 version of ONEDANT that contains linear-discontinuous spatial differencing [ONET], S2 synthetic acceleration [LJL3], Galerkin quadrature [MOR5], and a new angular differencing scheme for curvilinear geometries [MOR6]. In the remainder of this report, we shall refer to this version of ONEDANT as ONEDANT-LD. The input and output of ONEDANT-LD is the same as that described in earlier ONEDANT documentation [ONED].

Three reference documents have been written to aid the user of the CEPXS/ONEDANT-LD code package: a User's Guide, a Physics Guide, and a Results Guide. The User's Guide describes the operation of the CEPXS/ONEDANT-LD code package. The Results Guide provides an extensive set of examples that illustrates the variety of calculations that are possible with CEPXS/ONEDANT-LD.

This document is the Physics Guide. In the first chapter, the multigroup-Legendre cross sections produced by CEPXS are reviewed. The following chapters examine the cross sections for specific interactions in greater detail. Approximations that are unique to electrons (and positrons), such as the extended transport correction and the restricted continuous slowing-down approximation, are explained. In Appendix A, sections of the CEPXS code that relate to specific cross sections are identified.

The cross-section generating code, CEPXS, was devised to meet two goals:

(1) The cross sections produced by CEPXS enable coupled electron-photon transport calculations to be performed with the standard discrete ordinates code, ONEDANT-LD. Standard discrete ordinates codes solve the Boltzmann transport equation [BELL] for all types of particles. For instance, such discrete ordinates codes can be used for both neutron and gamma transport calculations. While the Boltzmann transport equation also applies to the transport of electrons in field-free environments without collective (non-linear) effects, discrete ordinates codes are ill-suited for solving the Boltzmann transport equation for electrons. The numerical reasons for these difficulties are discussed in the next chapter. However, CEPXS constructs special electron multigroup-Legendre cross sections that enable a Boltzmann transport solver like ONEDANT-LD to effectively solve the more amenable Boltzmann-CSD transport equation [MOR2, BART] for electrons.

(2) CEPXS models the same physical interactions as Version 2.1 of ITS code package. The Integrated-TIGER-Series [ITS] code package consists of state-of-the art coupled electron-photon Monte Carlo codes. Many of the same physical models are used in both CEPXS and ITS. Materials of

arbitrary composition can be specified by the user of either code. The electron-photon cascade is modelled over a similar energy range in the two codes. Electron cross sections are not generally available at low energies (below one kev) for materials of arbitrary composition. Hence, the transport of particles below one keV is not allowed by either code. The maximum particle energy by CEPXS is 100 MeV.

I.2 COMPOUNDS

The cross section of a compound material can be expressed as a combination of the cross sections of its constituent elements. Consider the following cross sections:

σ $\equiv$ Macroscopic cross section of an element in units of cm^2/g

σ_{mol} $\equiv$ Macroscopic cross section of a compound in units of cm^2/g

ξ $\equiv$ Microscopic cross section of an element in units of $cm^2/atom$

ξ_{mol} $\equiv$ Microscopic cross section of a compound in units of $cm^2/molecule$

A microscopic cross section is related to the probability of interaction per atom (or per molecule.) Microscopic cross sections are expressed in units of area and are related to their macroscopic counterparts by:

$$\sigma = \frac{N_A \xi}{A} \quad , \quad \sigma_{mol} = \frac{N_A \xi_{mol}}{A_{mol}} \tag{I.4}$$

where N_A is Avogardo's number, A is the gram-atomic weight of an element and A_{mol} is the gram-molecular weight of a molecule. The microscopic cross section of a molecule is defined as:

$$\xi_{mol} = \sum_i N_i \, \xi_i \tag{I.5}$$

where N_i is the number fraction of the ith element in the compound (i.e. the number of atoms per molecule.) Hence, the macroscopic cross section of a compound can be expressed as a combination of the macroscopic cross sections of the constituent elements:

$$\sigma_{mol} = \frac{N_A \xi_{mol}}{A_{mol}} = \sum_i N_i \frac{A_i}{A_{mol}} \sigma_i = \sum_i w_i \, \sigma_i \tag{I.6}$$

where w_i is the weight fraction of the ith element in the compound. In CEPXS, most cross sections for compounds can be constructed according to Eq. I.6. However, the collisional stopping power of a compound is not merely a combination of elemental stopping powers.

I.3 THE MULTIGROUP-LEGENDRE APPROXIMATION

The multigroup method [BELL] involves a discretization of the particle energy domain into energy intervals or groups:

$$
\begin{array}{c|c|c|c|c|}
 & \text{group 1} & \text{group 2} & \circ \circ \circ \circ & \text{group G} \\
\hline
E_1 & & E_2 & E_3 & E_G \qquad E_{G+1}
\end{array}
$$

where $E_1 > E_2 > E_3 > \circ \circ \circ E_{G+1}$ and E_{G+1} is the cutoff energy. By convention, the higher group numbers are associated with lower particle energies.

In CEPXS, different group structures may be selected for photons and electrons. However, the energy domain must be the same for all particles. That is, the cutoff energy, E_{G+1}, and the upper boundary energy, E_1, must be the same for both electrons and photons.

In the multigroup approximation, all particles in the same energy group are assumed to interact with the same probability. The multigroup approximation is realistic only if the cross sections do not vary greatly in energy within a group. Hence, the structure of the energy grid can impact the accuracy of a prediction. For instance, the photoelectric cross section for an electron whose energy is slightly greater then a shell binding energy is significantly different than the photoelectric cross section for an electron whose energy is slightly less than that binding energy. In order to calculate the distribution of photoelectrons accurately, the group structure cannot be coarse in the vicinity of the shell binding energies.

The multigroup angular flux, $\psi_g(r,\Omega)$, is defined as:

$$
\psi_g(r,\Omega) = \int_{E_{g+1}}^{E_g} dE \; \psi(r,\Omega,E) \tag{I.7}
$$

where $\psi(r,\Omega,E)$ is the angular flux. The multigroup scalar flux is defined as:

$$\phi_g(r) = \frac{1}{4\pi} \int d\Omega \; \psi_g(r,\Omega) \qquad (I.8)$$

The differential cross section, $\sigma(r,E \rightarrow E',\mu)$, can be represented by a Legendre expansion:

$$\sigma(r,E \rightarrow E',\mu) = \sum_{L=0}^{\infty} \frac{2L+1}{4\pi} \sigma_L(r,E \rightarrow E') \; P_L(\mu) \qquad (I.9)$$

where:

$$\sigma_L(r,E \rightarrow E') = \int d\Omega \; P_L(\mu) \; \sigma(r,E \rightarrow E',\mu)$$
$$= 2\pi \int_{-1}^{1} d\mu \; P_L(\mu) \; \sigma(r,E \rightarrow E',\mu) \qquad (I.10)$$

In CEPXS, the Legendre expansion represented by Eq. I.9 is truncated at a finite order.

CEPXS does not treat the spatial variations of the cross section due to material heterogenities. Such variations are represented in ONEDANT [ONED] and will not be discussed here. In the remainder of this report, the spatial dependence of the cross sections will be ignored.

The multigroup-Legendre expansion coefficients for the cross sections that describe scattering and production interactions are stored by CEPXS in transfer matrices. For a differential cross section, the expansion coefficients that are stored in the transfer matrix of Lth-order are:

$$\sigma_{g \rightarrow g',L} = \frac{\int_{E_{g+1}}^{E_g} dE \; W(E) \int_{E_{g'+1}}^{E_{g'}} dE' \; \sigma_L(E \rightarrow E')}{\int_{E_{g+1}}^{E_g} dE \; W(E)} \qquad (I.11)$$

where $W(E)$ is the multigroup weighting function. In the above notation, the row index of the transfer matrix is (g) and the column index of the transfer matrix is (g'). Except where noted in this report, numerical quadrature techniques are used in CEPXS to evaluate these multigroup-Legendre expansion coefficients.

Since a weighting function must be arbitrarily chosen, a unique set of

multigroup cross sections does not exist. In CEPXS, a weighting function of zero-th order in energy is generally used to construct the multigroup cross sections. This function is piece-wise constant in energy:

$$W(E) = c_g \quad \text{for } E_g \geq E \geq E_{g+1} \tag{I.12}$$

where c_g is a group-dependent constant.

Hence the multigroup-Legendre expansion coefficients become:

$$\sigma_{g \rightarrow g',L} = \frac{\displaystyle\int_{E_{g+1}}^{E_g} dE \int_{E_{g'+1}}^{E_{g'}} dE' \; \sigma_L(E \rightarrow E')}{\Delta E_g} \tag{I.13}$$

where $\Delta E_g = E_g - E_{g+1}$

I.4 THE COUPLED ELECTRON-PHOTON BOLTZMANN TRANSPORT EQUATIONS

The coupled Boltzmann equations [BELL] for the transport of the particles in the coupled electron-photon cascade are:

$$\Omega \bullet \nabla \psi^e + \Sigma_t^e \; \psi^e = \int dE' \int d\Omega' \; \Sigma^{ee}(E' \rightarrow E, \Omega' \rightarrow \Omega) \; \psi^e(r,E',\Omega')$$

$$+ \int dE' \int d\Omega' \; \Sigma^{\gamma e}(E' \rightarrow E, \Omega' \rightarrow \Omega) \; \psi^\gamma(r,E',\Omega')$$

$$+ \int dE' \int d\Omega' \; \Sigma^{pe}(E' \rightarrow E, \Omega' \rightarrow \Omega) \; \psi^p(r,E',\Omega')$$

$$\tag{I.14}$$

$$\Omega \bullet \nabla \psi^\gamma + \Sigma_t^\gamma \; \psi^\gamma = \int dE' \int d\Omega' \; \Sigma^{\gamma\gamma}(E' \rightarrow E, \Omega' \rightarrow \Omega) \; \psi^\gamma(r,E',\Omega')$$

$$+ \int dE' \int d\Omega' \; \Sigma^{e\gamma}(E' \rightarrow E, \Omega' \rightarrow \Omega) \; \psi^e(r,E',\Omega')$$

$$+ \int dE' \int d\Omega' \; \Sigma^{p\gamma}(E' \rightarrow E, \Omega' \rightarrow \Omega) \; \psi^p(r,E',\Omega')$$

$$\Omega \bullet \nabla \psi^p + \Sigma_t^p \; \psi^p = \int dE' \int d\Omega' \; \Sigma^{pp}(E' \rightarrow E, \Omega' \rightarrow \Omega) \; \psi^p(r,E',\Omega')$$

$$+ \int dE' \int d\Omega' \; \Sigma^{\gamma p}(E' \rightarrow E, \Omega' \rightarrow \Omega) \; \psi^\gamma(r,E',\Omega')$$

where:

$\psi^e(r,E,\Omega)$ $\quad$ = The electron angular flux,

$\psi^\gamma(r,E,\Omega)$ $\quad$ = The photon angular flux,

$\psi^p(r,E,\Omega)$ $\quad$ = The positron angular flux,

$\Sigma_t^e(r)$ $\quad$ = Total cross sections for electron interactions.

$\Sigma_t^\gamma(r)$ $\quad$ = Total cross section for photon interactions,

$\Sigma_t^p(r)$ $\quad$ = Total cross section for positron interactions,

$\Sigma^{ee}(E'\to E,\Omega'\to\Omega)$ $\quad$ = The electron-to-electron differential cross section,

$\Sigma^{\gamma e}(E'\to E,\Omega'\to\Omega)$ $\quad$ = The photon-to-electron differential cross section

$\Sigma^{pe}(E'\to E,\Omega'\to\Omega)$ $\quad$ = The positron-to-electron differential cross section,

$\Sigma^{\gamma\gamma}(E'\to E,\Omega'\to\Omega)$ $\quad$ = The photon-to-photon differential cross section

$\Sigma^{e\gamma}(E'\to E,\Omega'\to\Omega)$ $\quad$ = The electron-to-photon differential cross section

$\Sigma^{p\gamma}(E'\to E,\Omega'\to\Omega)$ $\quad$ = The positron-to-photon differential cross section

$\Sigma^{pp}(E'\to E,\Omega'\to\Omega)$ $\quad$ = The positron-to-positron differential cross section

$\Sigma^{\gamma p}(E'\to E,\Omega'\to\Omega)$ $\quad$ = The photon-to-positron differential cross section (pair production),

The boundary conditions which specify the source distribution are not included in Eq. I.14. The cross sections, Σ, that are appear in the Boltzmann transport equation are aggregate cross sections that are assembled from the macroscopic cross sections for several interactions.

I.5 AGGREGATE TRANSFER MATRICES

CEPXS constructs multigroup-Legendre transfer matrices for each of the eight aggregate differential cross sections that appear in the coupled Boltzmann transport equations. A variety of production and scattering interactions contribute to each of these aggregate transfer matrices.

The aggregate electron-to-electron transfer matrix includes collisional scattering (C), knock-on production (K), radiative scattering (B), elastic scattering (E), and Auger production following impact ionization (IE):

$$\Sigma^{ee}_{g \to g',L} = \sigma^{C}_{g \to g',L} + \sigma^{K}_{g \to g',L} + \sigma^{B}_{g \to g',L} + \sigma^{E}_{g \to g',L} + \sigma^{IE}_{g \to g',L} \qquad (I.15)$$

In the above equation, and in the remainder of this report, the group indices for different particle species will be denoted with specific symbols. Namely, (g),(f),(h) denote electron groups, photon groups, and positron groups, respectively. The symbol (k) will be used to denote group indices irrespective of particle type.

The aggregate electron-to-photon transfer matrix includes bremsstrahlung production (BP) and fluorescence production following impact ionization (IF):

$$\Sigma^{e\gamma}_{g \to f,L} = \sigma^{BP}_{g \to f,L} + \sigma^{IF}_{g \to f,L} \qquad (I.16)$$

The aggregate photon-to-photon transfer matrix includes incoherent scattering (KN) and fluorescence production following photoionization (PIF):

$$\Sigma^{\gamma\gamma}_{f \to f',L} = \sigma^{KN}_{f \to f',L} + \sigma^{PIF}_{f \to f',L} \qquad (I.17)$$

The aggregate photon-to-electron transfer matrix includes Compton electron production (CO), photoelectric production (PE), pair electron production (P-), and Auger production following photoionization (PIE).

$$\Sigma^{\gamma e}_{f \to g,L} = \sigma^{CO}_{f \to g,L} + \sigma^{PE}_{f \to g,L} + \sigma^{PIE}_{f \to g,L} + \sigma^{P-}_{f \to g,L} \qquad (I.18)$$

The aggregate photon-to-positron transfer matrix consists solely of pair positron production (P+):

$$\Sigma^{\gamma p}_{f \to h,L} = \sigma^{P+}_{f \to h,L} \qquad (I.19)$$

The aggregate positron-to-positron transfer matrix includes collisional scattering (C), radiative scattering (B), and elastic scattering (E):

$$\Sigma^{pp}_{h \to h',L} = \sigma^{C}_{h \to h',L} + \sigma^{B}_{h \to h',L} + \sigma^{E}_{h \to h',L} \qquad (I.20)$$

The aggregate positron-to-photon transfer matrix includes

bremsstrahlung production (BP), fluorescence production following impact ionization (IF), and annihilation radiation (ANN):

$$\Sigma^{p\gamma}_{h\rightarrow f,L} = \sigma^{BP}_{h\rightarrow f,L} + \sigma^{IF}_{h\rightarrow f,L} + \sigma^{ANN}_{h\rightarrow f,L} \qquad (I.21)$$

The aggregate positron-to-electron transfer matrix includes knock-on production and (K) Auger production following impact ionization (IE):

$$\Sigma^{pe}_{h\rightarrow g,L} = \sigma^{K}_{h\rightarrow g,L} + \sigma^{IE}_{h\rightarrow g,L} \qquad (I.22)$$

I.6 AGGREGATE REACTION CROSS SECTIONS

The aggregate total reaction cross sections, Σ_t, also appear in the coupled Boltzmann transport equations. The total cross section is one of several reaction cross sections that can be specified for each interaction. These reaction cross sections are denoted by $\sigma_{X,k}$ where the symbol X refers to the reaction type. The five different types of reaction cross sections assembled by CEPXS are: total (σ_t), absorption (σ_a), secondary production (σ_S), energy deposition (σ_E), and charge deposition (σ_C).

Multigroup reaction cross sections are calculated by CEPXS for each of these reaction types. The multigroup reaction rate is:

$$\sigma_{X,k}\,\phi_k(r) \qquad (I.23)$$

the reaction rate over all groups is:

$$\sum_{k=1}^{K} \sigma_{X,k}\,\phi_k(r) \qquad (I.24)$$

For instance, the energy (charge) deposition cross section can be used to calculate the total energy (charge) deposition profile.

Total multigroup cross sections are defined as the probability per unit pathlength that particles in a group interact. For scattering interactions which are represented by the differential cross section, σ^S, the total multigroup cross sections are:

$$\sigma_{t,k}^{S} = \frac{\int_{E_{k+1}}^{E_k} dE \int_{E_{min}}^{E} dE' \; \sigma_0^S(E \rightarrow E')}{\Delta E_k} \qquad (I.25)$$

where we have assumed that:

$$\sigma_0^S(E \rightarrow E') = 0 \quad \text{for } E' < E_{min}$$

Note that:

$$\sigma_{t,k}^{S} = \sum_{k'=1}^{K} \sigma_{k \rightarrow k',0}^{S}$$

only if $E_{min} \geq E_{K+1}$.

For absorption interactions which are represented by the non-differential cross section, σ^A, the total multigroup cross sections are:

$$\sigma_{t,k}^{A} = \frac{\int_{E_{k+1}}^{E_k} dE \; \sigma^A(E)}{\Delta E_k} \qquad (I.26)$$

Since particle production occurs in conjunction with either particle scattering or particle absorption, the differential production cross section does not contribute to the total reaction cross section.

The aggregate total multigroup cross sections calculated by CEPXS are:

$$\Sigma_{t,g}^{e} = \sigma_{t,g}^{C} + \sigma_{t,g}^{B} + \sigma_{t,g}^{E}$$

$$\Sigma_{t,f}^{\gamma} = \sigma_{t,f}^{KN} + \sigma_{t,f}^{PA} + \sigma_{t,f}^{PPA} \qquad (I.27)$$

$$\Sigma_{t,h}^{P} = \Sigma_{t,g}^{e} \qquad \text{for } h = g$$

where the macroscopic cross sections associated with collisional scattering (C), radiative scattering (B), elastic scattering (E), incoherent scattering (KN), photoelectric absorption (PA) and pair interaction absorption (PAA) are identified. Note that the total cross section for positrons is identical to the total cross section for

electrons. In CEPXS, the same group structure is used for both positrons and electrons.

In a scattering interaction, particles are not physically absorbed. However, particles can be effectively absorbed if the scattered particle's energy is less than the cutoff energy. The effective absorption multigroup cross section is defined as the number of particles in a group that scatter into energies below cutoff, per unit pathlength:

$$\sigma^S_{a,k} = \sigma^S_{t,k} - \sum_{k'=1}^{K} \sigma^S_{k \to k',0} \qquad (I.28)$$

If the scattered particles never acquire energy less than the cutoff energy ($E_{min} > E_{K+1}$), the effective absorption cross sections are identically zero.

For absorption interactions:

$$\sigma^A_{a,k} = \sigma^A_{t,k} \qquad (I.29)$$

The aggregate absorption multigroup cross sections calculated by CEPXS are:

$$\Sigma^e_{a,g} = \sigma^C_{a,g} + \sigma^B_{a,g}$$

$$\Sigma^\gamma_{a,f} = \sigma^{KN}_{a,f} + \sigma^{PA}_{a,f} + \sigma^{PPA}_{a,f} \qquad (I.30)$$

$$\Sigma^P_{a,h} = \Sigma^e_{a,g} \qquad \text{for} \quad h = g$$

Secondary production cross sections are defined as the number of particles produced, per unit pathlength, due to particles in a group. These reaction cross sections are defined only for production interactions. If the differential production cross section is denoted by σ^P, the secondary production cross sections are defined as:

$$\sigma^P_{S,k} = \sum_{k'=1}^{K} \sigma^P_{k \to k',0} \qquad (I.31)$$

The aggregate secondary production cross sections calculated by CEPXS are:

$$\Sigma_{S,g}^{e} = \sigma_{S,g}^{K} + \sigma_{S,g}^{BP} + \sigma_{S,g}^{IE} + \sigma_{S,g}^{IF}$$

(I.32)

$$\Sigma_{S,f}^{\gamma} = \sigma_{S,f}^{CO} + \sigma_{S,f}^{PE} + \sigma_{S,f}^{PIE} + \sigma_{S,f}^{PIF} + \sigma_{S,f}^{P+} + \sigma_{S,f}^{P-}$$

$$\Sigma_{S,h}^{p} = \Sigma_{S,g}^{e} + \sigma_{S,h}^{ANN} \quad \text{for} \quad h = g$$

for the following production interactions: bremsstrahlung (BP), knock-on (K), Compton electron (CO), photoelectron (PE), fluorescence following impact ionization (IF) and photoionization (PIF), Auger following impact ionization (IE) and photoionization (PIE), pair electron (P-) and pair positron (P+), and annihilation (ANN).

Energy-deposition cross sections are associated with every type of interaction. These "cross sections" are defined as the net energy deposited in the medium due to the interactions of particles in a group per unit pathlength. Such cross sections have units of energy per distance. The energy-deposition multigroup cross sections for a scattering interaction could be calculated in the following fashion:

(I.33)

$$\sigma_{E,k}^{S} = \frac{\displaystyle\int_{E_{k+1}}^{E_{k}} dE \int_{E_{min}}^{E} dE'\, E\, \sigma_{0}^{S}(E \to E') - \int_{E_{k+1}}^{E_{k}} dE \int_{E_{K+1}}^{E} dE'\, E'\, \sigma_{0}^{S}(E \to E')}{\Delta E_{k}}$$

However, in CEPXS, we chose to define an "effective" multigroup energy deposition cross sections using the group mid-point energies:

$$\sigma_{E,k}^{S} = \sigma_{t,k}^{S}\left(E_{k}^{m}\right) - \sum_{k'=1}^{K} \sigma_{k \to k',0}^{S}\left(E_{k'}^{m}\right)$$

(I.34)

where:

E_{k}^{m} is the midpoint energy of group k.

In the limit of increasing number of groups, the effective energy deposition cross sections become equivalent to the energy deposition cross sections defined by Eq. I.33.

A production interaction involves the removal of energy from the site of

the interaction. Hence, the effective energy deposition cross sections
for production interactions are:

$$\sigma_{E,k}^{P} = -\sum_{k'=1}^{K} \sigma_{k \to k',0}^{P} \left(E_{k'}^{m} \right) \tag{I.35}$$

Since an absorption interaction results in the deposition of energy, the
effective energy deposition cross sections for such interactions are:

$$\sigma_{E,k}^{A} = \sigma_{a,k}^{A} \left(E_{k}^{m} \right) \tag{I.36}$$

The aggregate energy deposition cross sections calculated by CEPXS are:

$$\Sigma_{E,g}^{e} = \sigma_{E,g}^{C} + \sigma_{E,g}^{B} + \sigma_{E,g}^{IE} + \sigma_{E,g}^{IF} + \sigma_{E,g}^{K} + \sigma_{E,g}^{BP} \tag{I.37}$$

$$\Sigma_{E,f}^{\gamma} = \sigma_{E,f}^{KN} + \sigma_{E,f}^{CO} + \sigma_{E,f}^{PE} + \sigma_{E,f}^{PA} + \sigma_{E,f}^{PIF} + \sigma_{E,f}^{PIE} + \sigma_{E,f}^{PPA} + \sigma_{E,f}^{P-} + \sigma_{E,f}^{P+}$$

$$\Sigma_{E,h}^{P} = \Sigma_{E,g}^{e} + \sigma_{E,h}^{ANN} \quad \text{for} \quad h = g$$

The "charge" deposition cross sections are defined as the net number of
electrons deposited in the medium due to the interactions of particles
in a group per unit pathlength. A positive charge deposition cross
section corresponds to electron deposition while a negative charge
deposition cross section corresponds to electron removal.

For scattering and absorption interactions, these cross sections are:

$$\sigma_{C,k}^{S} = \sigma_{a,k}^{S} \, q(k)$$

$$\sigma_{C,k}^{A} = \sigma_{a,k}^{A} \, q(k) \tag{I.38}$$

where:

$$q(k) = 1 \text{ if } k \text{ is an electron group}$$
$$= -1 \text{ if } k \text{ is a positron group}$$
$$= 0 \text{ if } k \text{ is a photon group} \quad .$$

For production interactions, the charge deposition cross sections are:

$$\sigma_{C,k}^{P} = -\sum_{k'=1}^{K} \sigma_{k \to k',0}^{P} \, q(k') \qquad\qquad (I.39)$$

The aggregate multigroup charge deposition cross sections calculated by CEPXS are:

$$\Sigma_{C,g}^{e} = \sigma_{C,g}^{C} + \sigma_{C,g}^{B} + \sigma_{C,g}^{K} + \sigma_{C,g}^{IE}$$

$$\Sigma^{\gamma} = \sigma_{C,f}^{CO} + \sigma_{C,f}^{PE} + \sigma_{C,f}^{PIE} \qquad\qquad (I.40)$$

$$\Sigma_{C,h}^{e} = -\sigma_{C,g}^{C} - \sigma_{C,g}^{B} + \sigma_{C,g}^{K} + \sigma_{C,g}^{IE} \qquad \text{for } h = g$$

I.7 PARTICLE CONSERVATION

In order for particles to be conserved, the multigroup-Legendre cross sections produced by CEPXS must satisfy:

$$\Sigma_{a,k} = \Sigma_{t,k} + \Sigma_{S,k} - \sum_{\text{all } k'} \Sigma_{k \to k',0} \qquad\qquad (I.41)$$

for all groups.

If the above equation is not satisfied in any group, the number of particles in a CEPXS/ONEDANT calculation will not be conserved. CEPXS will abort the calculation if the left-hand side of the above equation differs from the right-hand side by more than .01 %. This check was especially useful during the development of CEPXS to insure that new interactions were added to the code in a consistent fashion.

II. INELASTIC COLLISIONAL SCATTERING
AND KNOCK-ON PRODUCTION

II.1 THE BOLTZMANN-CSD EQUATIONS

The electron Boltzmann transport equation is not amenable to a standard discrete ordinates solution. This is because an accurate multigroup representation of the collisional cross section for electrons, σ^C, is impractical. Since this inelastic cross section rapidly increases as energy loss become small, an accurate multigroup representation would require that an excessive number of narrow-width groups be used. This would make the cost of a discrete ordinates solution exorbitant.

In order to use the multigroup approach, an alternate treatment of electron inelastic interactions is required. Inelastic interactions (both collisional and radiative) can be divided into two classes: "catastrophic" interactions that result in large-energy losses and "soft" interactions that result in small-energy losses. Catastrophic interactions are represented by macroscopic cross sections for which a conventional multigroup treatment is practical.

A different approach is required for soft interactions. The cumulative effect of many soft interactions can be approximated by the continuous energy loss of an electron without angular deflection. This is the restricted continuous slowing-down (CSD) approximation. In the context of this approximation, the electron flux satisfies the Boltzmann-CSD equation [BART]. If all inelastic interactions (both collisional and radiative) are divided into soft and catastrophic events and the CSD approximation is applied to the former, the coupled electron-photon transport equations become:

$$\Omega \cdot \nabla \psi^e + \Sigma_t^e \, \psi_e = \int dE' \int d\Omega' \; \Sigma_*^{ee}(E' \rightarrow E, \Omega' \rightarrow \Omega) \; \psi^e(E', \Omega')$$

$$+ \frac{\partial}{\partial E}\left[R_e^C(E) \; \psi^e(E, \Omega) \right] + \frac{\partial}{\partial E}\left[R_e^B(E) \; \psi^e(E, \Omega) \right]$$

$$+ \int dE' \int d\Omega' \; \Sigma^{\gamma e}(E' \rightarrow E, \Omega' \rightarrow \Omega) \; \psi^\gamma(E', \Omega')$$

$$+ \int dE' \int d\Omega' \; \Sigma^{pe}(E' \rightarrow E, \Omega' \rightarrow \Omega) \; \psi^p(E', \Omega')$$

$$\text{(II.1)}$$

$$\Omega \cdot \nabla \psi^\gamma + \Sigma_t^\gamma \, \psi^\gamma = \int dE' \int d\Omega' \; \Sigma^{\gamma\gamma}(E' \to E, \Omega' \to \Omega) \; \psi^\gamma(E', \Omega')$$

$$+ \int dE' \int d\Omega' \; \Sigma^{e\gamma}(E' \to E, \Omega' \to \Omega) \; \psi^e(E', \Omega')$$

$$+ \int dE' \int d\Omega' \; \Sigma^{P\gamma}(E' \to E, \Omega' \to \Omega) \; \psi^P(E', \Omega')$$

$$\Omega \cdot \nabla \psi^P + \Sigma_t^P \, \psi^P = \int dE' \int d\Omega' \; \Sigma_*^{PP}(E' \to E, \Omega' \to \Omega) \; \psi^P(E', \Omega')$$

$$+ \frac{\partial}{\partial E}\Big[\, R_p^C(E) \; \psi^P(E,\Omega) \, \Big] + \frac{\partial}{\partial E}\Big[\, R_p^C(E) \; \psi^P(E,\Omega) \, \Big]$$

$$+ \int dE' \int d\Omega' \; \Sigma^{\gamma P}(E' \to E, \Omega' \to \Omega) \; \psi^\gamma(E', \Omega')$$

where:

$\Sigma_*^{ee}(E' \to E, \Omega' \to \Omega)$ = The electron-to-electron differential cross section that does not include soft inelastic interactions

$\Sigma_*^{PP}(E' \to E, \Omega' \to \Omega)$ = The positron-to-positron differential cross section that does not include soft inelastic interactions

$R_e^C(E)$ = The restricted collisional stopping power for electrons

$R_e^B(E)$ = The restricted radiative stopping power for electrons

$R_p^C(E)$ = The restricted collisional stopping power for positrons

$R_p^B(E)$ = The restricted radiative stopping power for positrons

The Boltzmann-CSD transport equation can be derived from the Boltzmann transport equation in a manner analogous to the derivation of the Fokker-Planck transport equation [MOR2]. The term in the electron Boltzmann-CSD transport equation that contains the restricted stopping power (which will be defined later in this chapter) represents the continuous slowing-down of the electron due to soft interactions. Standard discrete ordinates codes like ONEDANT-LD are general Boltzmann transport solvers that lack explicit representation of the CSD operator.

There are two ways to represent the restricted CSD approximation in

discrete ordinates codes. The restricted CSD operator could be differenced directly in the solver routine of the discrete ordinates code [BART]. The disadvantage of this approach is that new discrete ordinates codes must be devised.

In CEPXS, we use the approach devised by Morel [MOR2], [MOR3] in which "pseudo" multigroup-Legendre cross sections are devised to represent the differenced form of the restricted CSD operator. These CSD cross sections are "unreal" to the extent that they do not have a microscopic counterpart. However these CSD cross sections enable a standard Boltzmann transport code like ONEDANT-LD to obtain real physical solutions to the Boltzmann-CSD equation.

The disadvantage of this approach is that artificial or numerical energy-loss straggling can occur. Energy-loss straggling refers to variations in energy loss that are not CSD. Hence, in the restricted CSD model, soft inelastic interactions should not exhibit energy-loss straggling. However, numerical energy-loss straggling can be associated with such interactions if the CSD cross sections do not represent a differenced form of the CSD operator of sufficiently high order. In CEPXS, the CSD cross sections are equivalent to a second-order diamond-differenced form of the restricted CSD operator [MOR3]. While such cross sections greatly suppress numerical energy-loss straggling, they do not eliminate it entirely. Differencing schemes that are of greater accuracy are difficult to implement in standard discrete ordinates codes [LAZO].

The CSD cross sections are devised for both soft collisions, σ^{SC}, and soft radiative scattering interactions, σ^{SB}. The electron-to-electron transfer matrices for collisional and radiative interactions can be defined in terms of these CSD cross sections:

$$\sigma^{C}_{g \to g',L} = \sigma^{CC}_{g \to g',L} + \sigma^{SC}_{g \to g',L}$$

$$\sigma^{B}_{g \to g',L} = \sigma^{CB}_{g \to g',L} + \sigma^{SB}_{g \to g',L}$$

(II.2)

where σ^{CC} is the catastrophic collisional cross section and σ^{CB} is the catastrophic radiative scattering cross section. Likewise, the collisional and radiative reaction cross sections can be represented by soft and catastrophic components:

$$\sigma^{C}_{X,g} = \sigma^{CC}_{X,g} + \sigma^{SC}_{X,g}$$

(II.3)

$$\sigma_{X,g}^{B} = \sigma_{X,g}^{CB} + \sigma_{X,g}^{SB}$$

When appropriate CSD cross sections are defined, the solution of the electron flux calculated by ONEDANT-LD is effectively the same as the solution of the Boltzmann-CSD equation for electrons. Positron inelastic interactions are treated in a similar fashion.

II.2 CATASTROPHIC COLLISIONAL SCATTERING

In CEPXS, inelastic scattering due to catastrophic collisions are modelled by the Moller microscopic cross section, ξ^{CC}. In contrast, ITS uses a condensed-history (multiple-event) model to account for the effect of inelastic collisions [BERG2]. Energy-loss straggling due to collisions must be explicitly introduced into the ITS model. This is not necessary in CEPXS since the differential Moller cross section properly accounts for the energy distribution of the particles after a catastrophic collision. However, since CEPXS uses the CSD approximation for soft collisions, there is no energy-loss straggling for these collisions.

One of the assumptions used in the derivation of the Moller cross section is that the incident electron collides with a free atomic electron (i.e. the binding energy of the atomic electron is neglected.) The adequacy of this assumption depends on how the energy of the incident electron compares to the binding energy of the atomic electron with which it collides. For instance, if the incident electron's energy is on the order of the binding energy of the K-shell electrons, the assumption of zero binding energy is inadequate for collisions with these electrons. However, this assumption would still be adequate for the collisions that involve the less tightly-bound electrons in the outer shells.

After an inelastic collision, two electrons emerge. By convention, the particle with the higher energy is considered to be the primary or scattered electron. The other particle is considered to be the knock-on electron. The differential Moller cross section determines the energy (and angular) distribution of both the primary and knock-on electron.

The Moller cross section [ZERBY] can be written as differential in the energy of the knock-on electron. The microscopic form of this cross section (in units of cm^2 per reduced electron energy) per collision with an atomic electron is:

$$\frac{d\xi^{CC}(T,\epsilon)}{d\epsilon} = \frac{2\pi r_0^2}{\beta^2} \left[\frac{1}{\epsilon^2} + \frac{1}{T_p^2} + \frac{1}{(T+1)^2} - \frac{(2T+1)}{(T+1)^2 \epsilon T_p} \right] \qquad (II.4)$$

where:

T ≡ Kinetic energy of the incident electron in units of reduced energy (or electron rest mass units),

T_p ≡ Kinetic energy of the scattered primary electron in units of reduced energy. T_p varies from $T/2$ to T by definition,

ϵ ≡ Energy lost by the incident electron in units of reduced energy. It is equivalent to the kinetic energy of the knock-on electron in reduced energy units. Since the knock-on energy is the difference between the energies T and T_p, ϵ varies from 0 to $T/2$,

β is the ratio of the electron's velocity to the speed of light, and r_0 is the classical electron radius defined in the glossary.

The macroscopic Moller cross section for a material is:

$$\frac{d\sigma^{CC}(T,\epsilon)}{d\epsilon} = \left(\frac{Z}{A}\right)_{eff} N_A \frac{d\xi^{CC}(T,\epsilon)}{d\epsilon} \qquad (II.5)$$

where the expression in brackets is defined in the glossary.

The angle, θ_p, at which the primary electrons emerge relative to the direction of the incident electron is given by kinematics:

$$\mu_p = \cos(\theta_p) = \left[\frac{T_p(T+2)}{T(T_p+2)} \right]^{1/2} \qquad (II.6)$$

These angles are highly forward peaked relative to the direction of the incident electron. For instance, the maximum angle at which a primary can emerge is:

$$\sin^2\theta_{max} = \frac{2}{T+4} \qquad (II.7)$$

In ITS, μ_p is assumed to be unity and the angular deflection of the primary electron is accounted for by a modification to the nuclear elastic scattering cross section [BERG2].

Because energy and angle are kinematically related, the Moller cross section that is differential in both energy and angle is:

$$\frac{d\sigma^{CC}}{dT_p d\Omega_p} = \frac{d\sigma^{CC}}{dT_p} \frac{1}{2\pi} \delta(\mu - \mu_p) \qquad (II.8)$$

The total cross section for a catastrophic collision is obtained by integrating the differential cross section over all possible energies and angles at which primary electrons can emerge. Because the Moller cross section is singular at $\epsilon = 0.0$, this integration must be truncated at a primary electron energy that corresponds to a non-zero knock-on energy, ϵ_{cc}:

$$\sigma_t^{CC}(T) = \int_{T/2}^{T-\epsilon_{cc}} dT_p \int d\Omega_p \frac{d\sigma^{CC}}{dT_p d\Omega_p} \qquad (II.9)$$

The energy, ϵ_{cc}, is the smallest energy that a knock-on electron is allowed to have <u>as a result of a catastrophic collision</u>. Collisions that produce primary electrons with energy less than $T-\epsilon_{cc}$ are called catastrophic. The energy (ϵ_{cc}) is chosen such that, in catastrophic collisions, primary electrons appear in energy groups that are non-adjacent to the energy group of the incident particle. For instance, for an electron with energy (T) in group (g), $\epsilon_{cc} = T - T_{g+2}$. Hence, ϵ_{cc} depends on both the kinetic energy of the incident electron <u>and</u> the group structure. While the energy, ϵ_{cc}, cannot be less than the smallest width of an electron energy group, it may be less than the cutoff energy.

The restriction of catastrophic collisions to transfer between non-adjacent energy groups is required to insure that, in a multigroup formulism, ϵ_{cc} is never zero. If scattering into adjacent energy groups were allowed, ϵ_{cc} would equal $T-T_{g+1}$. Since the kinetic energies of electrons in a group can assume any value between T_g and T_{g+1}, ϵ_{cc} could assume the value zero if catastrophic collisions into adjacent groups were allowed.

The total cross sections associated with catastrophic collisions are:

$$\sigma_{t,g}^{CC} = \frac{1}{\Delta T_g} \int_{T_{g+1}}^{T_g} dT \int_{T/2}^{T_{g+2}} dT_p \int d\Omega_p \frac{d\sigma^{CC}(T,T_p)}{dT_p d\Omega_p}$$

$$(II.10)$$

$$= \frac{1}{\Delta T_g} \int_{T_{g+1}}^{T_g} dT \int_{T/2}^{T_{g+2}} dT_p \frac{d\sigma^{CC}(T,T_p)}{dT_p}$$

In order to calculate the multigroup transfer matrices associated with catastrophic collisions, the group structure of the electrons must be considered. For instance, in order for electrons in group (g) to produce primaries in group (g‘), the highest energy of the lower energy group ($T_{g‘}$) must exceed the minimum energy of a primary electron ($T_{g+1}/2$.) For a catastrophic collision that involves a single atomic electron, the expansion coefficients of the Lth-order transfer matrix are:

FOR L = 0,1,...LMAX:

FOR g‘ = g+2, g+1, ... G:

$$\xi^{CC}_{g \to g‘,L} = \frac{1}{\Delta T_g} \int_{T_{g+1}}^{T_g} dT \int_{Max\left[T_{g‘+1} , \frac{T}{2} \right]}^{T_{g‘}} dT_p\ H(\Delta T_p)\ P_L(\mu_p) \frac{d\xi^{CC}(T,T_p)}{dT_p}$$

(II.11)

where $H(x)$ is a step function (see glossary) whose argument is:

$$\Delta T_p = T_{g‘} - Max\left[T_{g‘+1} , \frac{T}{2} \right]$$

and LMAX is the maximum order of the Legendre expansion.

The terms of the macroscopic transfer matrices for inelastic scattering are related to the terms of the microscopic transfer matrices by:

$$\sigma^{CC}_{g \to g‘,L} = \left(\frac{Z}{A}\right)_{eff} N_A\ \xi^{CC}_{g \to g‘,L}$$

(II.12)

Other reaction cross sections can be defined for inelastic collisions. The effective absorption cross sections due to catastrophic collisions are:

$$\sigma^{CC}_{a,g} = \sigma^{CC}_{t,g} - \sum_{g‘ > g} \sigma^{CC}_{g \to g‘,0}$$

(II.13)

The effective absorption cross section due to catastrophic collisions that involve incident electrons in group (g) is zero unless lowest primary electron energy $(T_{g+1}/2)$ is less than the cutoff energy.

The effective energy deposition cross sections due to catastrophic collisions are:

$$\sigma_{E,g}^{CC} = \sigma_{t,g}^{CC} E_g^m - \sum_{g' > g} \sigma_{g \to g',0}^{CC} E_{g'}^m \qquad (II.14)$$

while the charge deposition cross section due to catastrophic collisions are:

$$\sigma_{C,g}^{CC} = \sigma_{a,g}^{CC} \qquad (II.15)$$

II.3 KNOCK-ON ELECTRON PRODUCTION

Knock-on electrons are defined to be the least energetic electrons that emerge following an inelastic collision. In both ITS and CEPXS, the minimum energy that a knock-on electron can possess is the cutoff energy (T_{G+1}). Both codes use the Moller cross section differential in the knock-on energy to obtain the energy distribution of the knock-on electrons. However, the energies of the primary and knock-on electrons are not correlated (i.e. are not kinematically related) in ITS since the Moller cross section is not used to determine the energy distribution of the primary electrons.

A greater degree of correlation exists in CEPXS. Most of the primary electrons scattered in a catastrophic collision will be correlated in energy with a knock-on electron. However, the extent of this correlation is limited by the electron energy domain that is selected by the user of the code. For instance, if ϵ_{cc} is less than the cutoff energy, not every primary electron scattered in a catastrophic collision is associated with a knock-on electron.

An energy correlation does not exist between knock-on electrons and electrons that lose energy as a result of soft collisions. This is because, in the CSD approximation, individual soft collisions are not resolved. Nonetheless, if ϵ_{cc} is greater than the cutoff energy, those knock-ons that are generated with energy between T_{G+1} and ϵ_{cc} must be associated with soft collisions, even if a direct energy correlation is absent.

The Moller cross section neglects the binding energy of the atomic electrons. Since the impact ionization cross section depends on these binding energies, the relaxation radiation that is produced from impact ionization will not be correlated with electron energy loss in either CEPXS or ITS.

The angles at which the secondary electrons emerge are derived from kinematics. Like the primaries, such secondaries emerge in forward directions relative to the direction of travel of the incident electron. However, the angular distribution of the knock-ons is not as forward peaked as that of the primaries. The knock-on electrons emerge at an angle, θ_s, relative to the incident electron's direction:

$$\mu_s = \cos(\theta_s) = \left[\frac{\epsilon(T+2)}{T(\epsilon+2)} \right]^{1/2} \qquad (II.16)$$

The microscopic Moller cross section differential in the energy of the knock-on electron, ξ^K, associated with a collision with an atomic electron is given by:

$$\frac{d\xi^K}{d\epsilon d\Omega_s} = \frac{d\xi^K}{d\epsilon} \frac{1}{2\pi} \delta(\mu - \mu_s) \qquad (II.17)$$

In order for electrons in group (g) to produce knock-on electrons in group (g'), the lowest energy of the lower energy group $(T_{g'+1})$ must not exceed the maximum knock-on energy $(T_g/2.)$ The expansion coefficients of the Lth-order transfer matrix for knock-on electron production are:

FOR L = 0,1,...LMAX
FOR g' = g+2, g+3, ... G :

$$\xi^K_{g \to g',L} = \frac{1}{\Delta T_g} \int_{T_{g+1}}^{T_g} dT \int_{T_{g'+1}}^{Min\left[T_{g'}, \frac{T}{2} \right]} d\epsilon \; H[\Delta\epsilon] \; P_L(\mu_s) \; \frac{d\xi^K(T,\epsilon)}{d\epsilon}$$

$$(II.18)$$

where the argument of the step function is:

$$\Delta\epsilon = Min\left[T_{g'}, \frac{T}{2} \right] - T_{g'+1}$$

The macroscopic transfer matrices for knock-on production are:

$$\sigma^K_{g \to g',L} = \left(\frac{Z}{A}\right)_{eff} N_A \, \zeta^K_{g \to g',L}$$

(II.19)

The effective energy deposition cross sections due to knock-on production are:

$$\sigma^K_{E,g} = - \sum_{g' > g} \sigma^K_{g \to g',0} \, E^m_{g'}$$

(II.20)

The charge deposition cross sections due to knock-on production are:

$$\sigma^K_{C,g} = - \sum_{g' > g} \sigma^K_{g \to g',0}$$

(II.21)

while the secondary production cross sections due to knock-ons are:

$$\sigma^K_{S,g} = \sum_{g' > g} \sigma^K_{g \to g',0}$$

(II.22)

Knock-on production will not contribute to either the total or the absorption reaction rates.

II.4 SOFT COLLISIONAL SCATTERING

In CEPXS, the definition of a soft collisions depends on the multigroup energy grid. In a soft collision, a scattered electron appears in the energy group that is adjacent to the group associated with the incident electron. CEPXS does not model soft collisions with a single-event cross section since a multigroup representation of such a cross section is not feasible. Rather, the restricted CSD approximation is used for soft collisions. Hence, energy-loss straggling is not associated with soft collisions.

The expansion coefficients for the Lth-order transfer matrix associated with the first-order differenced form of the restricted CSD operator [MOR2] are:

FOR L = 0,1,...LMAX
FOR g = 1,2,...G-1:

$$\sigma^{SC}_{g\rightarrow g',L} = \frac{R^C(E^m_g)}{E^m_g - E^m_{g'}} \; \delta_{g'(g+1)} \qquad\qquad (II.23)$$

where:

R^C = Restricted collisional stopping power,

and

E^m_g = Midpoint energy of the group g.

In a soft collision, an electron is assumed to slow down without angular deflection. The angular distribution associated with the CSD cross sections is the delta function, $\delta(\mu-1)$, which must be represented by a truncated Legendre expansion in CEPXS:

$$\sigma^{SC}_{g\rightarrow g',L} = \sigma^{SC}_{g\rightarrow g',0} \qquad FOR \quad L = 0,1, \ldots LMAX \qquad\qquad (II.24)$$

In a discrete ordinates calculation, such a truncated representation of the delta function will cause artificial or numerical dispersion of the particles unless the proper quadrature set is chosen [MOR2] by the user who runs ONEDANT-LD. The proper quadrature set must be either Gaussian or Galerkin [MOR5], and must be of order LMAX+1.

The expansion coefficients of the Lth-order transfer matrix associated with the second-order (diamond-differenced) form of the restricted CSD operator [MOR3] are:

FOR L = 0,1,...LMAX
FOR g = 1,2,...G-1: $\qquad\qquad\qquad\qquad\qquad\qquad$ (II.25)

$$\sigma^{SC}_{g\rightarrow g',L} = \frac{(-1)^{g'-g+1}}{\Delta E_g} \; 2\left[R^C(E_{g'}) + R^C(E_{g'+1}) \right] \qquad IF \; G > g' > g$$

$$= \frac{(-1)^{G-g+1}}{\Delta E_g} \; 2\left[R^C(E_G) + S^C(E_{G+1}) \right] \qquad IF \; g' = G$$

$$= 0 \quad \text{OTHERWISE}$$

Note that the second-order CSD cross sections can be negative. This is possible since these cross sections do not have a microscopic counterpart. (While discrete ordinates codes can accept negative cross sections, such cross sections are not compatible with multigroup Monte Carlo codes.)

The effective absorption cross sections due to soft collisions are:

$$1^{st} \text{ order} \quad \begin{cases} \sigma^{SC}_{a,g} = 0 & \text{IF } g = 1, 2, \ldots G-1 \\[2mm] = \dfrac{R^C\left(E^m_g\right)}{E^m_g - E_u} & \text{IF } g = G \end{cases}$$

$$\text{(II.26)}$$

$$2^{nd} \text{ order} \quad \begin{cases} \sigma^{SC}_{a,g} = \dfrac{(-1)^{G-g}\, 2\, S^C(E_{G+1})}{\Delta E_g} & \text{FOR } g=1,2,\ldots G \end{cases}$$

where E_u is an arbitrary energy that is less than the cutoff energy [MOR2].

The total cross sections for soft collisions are:

$$1^{st} \text{ order} \quad \begin{cases} \sigma^{SC}_{t,g} = \sigma^{SC}_{a,g} + \sigma^{SC}_{g \to g+1,0} \end{cases}$$

$$2^{nd} \text{ order} \quad \begin{cases} \sigma^{SC}_{t,g} = \sigma^{SC}_{a,g} + \displaystyle\sum_{g' > g} \sigma^{SC}_{g \to g',0} \end{cases}$$

$$\text{(II.27)}$$

The energy deposition cross sections due to soft collisions are:

$$1^{st} \text{ order} \quad \begin{cases} \sigma^{SC}_{E,g} = 0 & \text{IF } g < G \\[2mm] = \sigma^{SC}_{a,g} E^m_g & \text{IF } g = G \end{cases}$$

$$\text{(II.28)}$$

$$2^{nd} \text{ order} \quad \begin{cases} \sigma^{SC}_{E,g} = \sigma^{SC}_{t,g} E^m_g - \displaystyle\sum_{g' > g} \sigma^{SC}_{g \to g',0}\, E^m_{g'} \end{cases}$$

These energy deposition cross sections are non-physical to the extent that they cannot be used to determine the amount of energy deposited by soft collisions involving electrons in a group (cf. Eq. I.23.) However,

they can be used to determine the total energy deposited by soft collisions involving electrons <u>in all groups</u> (cf. Eq. I.24.)

The charged deposition cross sections for soft collisions are:

$$\sigma^{SC}_{C,g} = \sigma^{SC}_{a,g} \qquad\qquad\qquad \text{(II.29)}$$

II.5 THE RESTRICTED COLLISIONAL STOPPING POWER

In order to construct the CSD cross sections described in the previous section, the restricted collisional stopping power must be known.

In the first-order scheme, the restricted stopping power must be evaluated at the midpoint energies of all electron groups except the last. The restricted collisional stopping power is defined as that portion of the total stopping power that is not due to catastrophic collisions:

FOR g = 1,2,...G-1: $\qquad\qquad\qquad\qquad\qquad\qquad\qquad\qquad$ (II.30)

$$R^C(E^m_g) = S^C(E^m_g) - \frac{m_e c^2}{\Delta T_g} \int_{T_{g+1}}^{T_g} dT \int_{T/2}^{T_{g+2}} dT_p \ H(\Delta T_p) \ (T-T_p) \ \frac{d\sigma^{CC}(T,T_p)}{dT_p}$$

where $S^C(E)$ is the total collisional stopping power (in units of MeV-cm^2/g) that is generally derived from Bethe theory [ICRU]. These total stopping powers are contained in the electron data set, DATAPAC [ETRAN] for each element from 1.0 GeV to 1.0 keV. The stopping power for a compound can be constructed with the aid of a density effect formulism discussed in the next section.

The restriction that the cutoff energy in both CEPXS and ITS cannot extend below 1.0 keV is due to the lack of stopping power data (as well as electron elastic scattering data) for arbitrary materials below one keV. Even for electron energies that exceed one keV, the Bethe stopping power theory can be inadequate in high-Z materials. Theoretical models of the stopping power at low energies must account for effects neglected in Bethe theory such as the inelastic scattering of electrons from conduction electrons, inner atomic electrons, and plasmons [SHIM].

Since the definitions of catastrophic and soft collisions are dependent on group parameters, the restricted stopping power that is calculated by CEPXS is also dependent on the electron group structure. As shown in

Fig. 1, the share of the total collisional stopping power that is associated with catastrophic collisions increases as more groups are selected. This is because the energy, ϵ_{cc}, that demarcates catastrophic and soft collisions decreases as the number of groups increases.

However, the figure indicates that soft collisions dominate collisional energy loss even when an excessive number of electron energy groups (160) are employed. Indeed, very many electron groups would be needed to make the collisional stopping power due to catastrophic collisions comparable to the total stopping power. This is another way of stating the previously mentioned assertion that an excessive number of groups would be required to accurately represent a single-event inelastic collisional cross section. In CEPXS, we are able to accurately calculate the energy loss of an electron due to inelastic scattering with only a modest number of groups ($\simeq$ 40) because the restricted CSD approximation is used to represent the energy loss that is due to soft collisions.

Both the total stopping power and the restricted collisional stopping power are defined to be positive. That is, a positive stopping power denotes the <u>loss</u> of energy per pathlength travelled. However, the restricted stopping power can become negative for low electron energies in high-Z materials if the total stopping power is derived from the Bethe theory. This is because the assumptions that are used to derive the Bethe stopping power are inadequate for low electron energies in high-Z materials. As shown in Fig. 2, the Bethe stopping power reaches a maximum value above one keV in tungsten. More accurate theoretical predictions [DEVA] indicate that the stopping power for electrons in tungsten is greatest for electrons with energy less than one keV.

In CEPXS, the Bethe stopping power is "corrected" at low energies in high-Z materials. (A comparable correction is not done in ITS.) Since a general formulism for electron stopping powers in arbitrary materials at low energies is not available (only ad hoc theoretical predictions are possible), a variety of empirical corrections have been proposed. In one such method, a parabolic extrapolation is applied to the stopping power at energies below the inflection point in the curve of stopping power versus energy [RAO]. In CEPXS, we employ a power-law extrapolation of the Bethe stopping power for each element below the arbitrarily selected energy of 10 keV:

$$S^C(E) = S^{Bethe}(E) \qquad\qquad \text{for } E > 10 \text{ keV}$$

$$S^C(E) = S^{Bethe}(10 \text{ keV}) \left[\frac{E(10 \text{ keV})}{E} \right]^x \qquad \text{for } E \leq 10 \text{ keV}$$

$$\text{where } x = - \left.\frac{\partial(\log S(E))}{\partial(\log(E))}\right|_{E = 10 \text{ keV}}$$

As shown in Fig. 2, this power-law extrapolation is in reasonable agreement with the stopping power in gold predicted by the more accurate theory. However, the Bethe stopping power is still adequate for lower-Z materials (Fig. 3.) The extrapolation exponents that are used in CEPXS are shown in Fig. 4 for all elements.

In order to evaluate the cross sections for the second-order differenced form of the CSD operator, the restricted stopping power must be evaluated at all group boundaries except the upper boundary, E_1, and the lower boundary, E_{G+1}. Since a boundary energy is both the top of one group and the bottom of another, there is some ambiguity as to how a catastrophic collision is to be defined for an electron whose energy is the same as that of a group boundary. For instance, if E_g is considered to be the upper boundary of group (g), a catastrophic collision would produce primary electrons with energies less than E_{g+2}. With this interpretation, the restricted collisional stopping power at energy E_g is:

FOR g = 2,3, ... G-1:

$$R_U^C(E_g) = S^C(E_g) - m_e c^2 \int_{T_g/2}^{T_{g+2}} dT_p \; H(\Delta T_p) \; (T_g - T_p) \; \frac{d\sigma^{CC}(T_g,T_p)}{dT_p} \qquad (II.32)$$

and

$$R_U^C(E_G) = 0$$

On the other hand, if E_g is considered to be the lower boundary of a group:

FOR g = 2,3, ... G:

$$R_L^C(E_g) = S^C(E_g) - m_e c^2 \int_{T_g/2}^{T_{g+1}} dT_p \; H(\Delta T_p) \; (T_g - T_p) \; \frac{d\sigma^{CC}(T_g,T_p)}{dT_p} \qquad (II.33)$$

In order to remove this ambiguity, we consider the restricted collisional stopping power at a group boundary to be the average of these two formulations:

FOR L = 0,1,...LMAX:
FOR g = 2,...G:

$$R^C(E_g) = \frac{1}{2} \left[R_U^C(E_g) + R_L^C(E_g) \right] \tag{II.34}$$

II.6 THE DENSITY EFFECT CORRECTION

Both ITS and CEPXS apply a density effect correction to the collisional
stopping power. The density arises from the self polarization of the
medium by the electron it effectively reduces the collisional stopping
power:

$$S^C(E) = \bar{S}^C(E) - \delta(E)$$

where δ is the density effect correction (in units of MeV-cm^2/g) and $\bar{S}^C$
is the uncorrected stopping power. The density effect correction
becomes most pronounced at high electron energies. For instance, in
water, the density effect correction becomes significant above one MeV
as shown in Fig. 5.

The stopping powers of a compound can be constructed from the
uncorrected stopping power of its constituent elements by:

$$S_{mol}^C(E) = \sum_i w_i \, \bar{S}_i^C(E) \quad - \quad \delta_{mol}(E) \tag{II.35}$$

if δ_{mol}, the density effect correction for the compound, is known.

A formula for the density effect correction for an arbitrary material
was devised by Sternheimer [STERN]. Both ITS and CEPXS use this
formulism:

$$\delta(T) = \frac{2\pi r_0^2 N_A m_e c^2}{\beta^2} \left(\frac{Z}{A}\right)_{eff} D(T) \tag{II.36}$$

where:

$$D(T) = 0.0 \qquad\qquad\qquad\qquad \text{IF } X \leq X_0$$
$$= 4.606*X + C + B*(X_1-X)^3 \quad \text{IF } X_0 < X \leq X_1$$
$$= 4.606*X + C \qquad\qquad\quad \text{IF } X > X1$$

$$X = LOG_{10}(P/m_e c)$$

$$P = \text{electron momentum}, \quad P/m_ec = [2T + T^2]^{1/2}$$

The parameters B and C are material dependent. For instance:

$$C = -2 \, \text{Log}(\bar{I}/h\nu_p) - 1 \quad ,$$

where:

(II.37)

$h\nu_p$ = Planck's constant times the plasma frequency in eV units

$$= 28.8 \left[\rho \left(\frac{Z}{A}\right)_{eff} \right]^{1/2} \quad ,$$

and

$\bar{I}$ = Effective mean ionization energy in eV units .

$$= Z \left(9.76 + 58.8 Z^{-1.19} \right) \quad \text{for } Z > 12,$$

$$= \text{Exp} \left[\sum_i \frac{w_i Z_i}{A_i} \text{Log}(I_i) \Big/ \left(\frac{Z}{A}\right)_{eff} \right] \quad \text{for a compound}$$

For a few elements ($Z \leq 12$), the mean ionization energy is tabulated in CEPXS.

The parameters, X_0 and X_1 depend on whether the material is a solid/liquid or a gas:

For a solid/liquid:

$$\bar{I} \geq 100 \text{ eV} \rightarrow X_1 = 3.0$$
$$X_0 = -.326C - 1.5 \quad \text{IF } -C \geq 5.215$$
$$= .2 \quad\quad\quad\quad\quad \text{OTHERWISE}$$

$$\bar{I} < 100 \text{ eV} \rightarrow X_1 = 2.0$$
$$X_0 = -.326C - 1.0 \quad \text{IF } -C \geq 3.681$$
$$= .2 \quad\quad\quad\quad\quad \text{OTHERWISE}$$

For a gas:

$$-C \geq 13.804 \rightarrow X_1 = 5.0, \quad X_0 = -.326C - 2.5$$
$$13.804 > -C \geq 12.250 \rightarrow X_1 = 5.0, \quad X_0 = 2.0$$
$$12.250 > -C \geq 11.500 \rightarrow X_1 = 4.0, \quad X_0 = 2.0$$
$$11.500 > -C \geq 11.000 \rightarrow X_1 = 4.0, \quad X_0 = 1.9$$

$$11.000 > -C \geq 10.500 \Rightarrow X_1 = 4.0, \quad X_0 = 1.8$$

$$10.500 > -C \geq 10.000 \Rightarrow X_1 = 4.0, \quad X_0 = 1.7$$

$$10.000 > -C \qquad \Rightarrow X_1 = 4.0, \quad X_0 = 1.6$$

The parameter, B, is:

$$B = \frac{- C - 4.606 X_0}{[\; X_1 - X_0 \;]^3}$$

III. INELASTIC RADIATIVE SCATTERING AND BREMSSTRAHLUNG PRODUCTION

Electrons can interact with both the electric field of the nucleus, and the electric field of the atomic electrons, to produce bremsstrahlung radiation. As was the case for inelastic collisions, CEPXS considers radiative energy loss to be of two different types: soft and catastrophic. While the bremsstrahlung cross section is used to characterize catastrophic events, soft radiative energy losses are treated by the restricted CSD approximation

III.1 THE BREMSSTRAHLUNG CROSS SECTION DIFFERENTIAL IN ENERGY

The bremsstrahlung production cross section is differential in both the energy and the emission angle of the photon. In CEPXS, this cross section is separated into a cross section that is differential in energy and a normalized differential angular distribution. The bremsstrahlung angular distribution is discussed in Section III.3. The bremsstrahlung cross section differential in energy that is used by CEPXS was devised by Berger and Seltzer [BERG1]. This bremsstrahlung cross section is assembled from a variety of Born approximation cross sections. It also includes empirical correction factors. ITS uses a more complex set of bremsstrahlung data. However, the same bremsstrahlung cross section that is used in CEPXS can be obtained in ITS if the SIMPLE-BREMS option is invoked by the user of ITS.

The macroscopic form of the bremsstrahlung production cross section differential in energy (in units of cm^2/g per reduced energy) that is suggested by Berger and Seltzer (for a single element) is:

$$\frac{d\sigma^{BP}(T,\epsilon)}{d\epsilon} = c_r(T) \ f_e(T,\epsilon) \left[\sigma_{3BN}(T,\epsilon) + \left[\sigma_{3BS}(T,\epsilon) - \sigma_{3BNb}(T,\epsilon) \right] \right.$$

$$\left. + w(T) \left[\sigma_{3CS}(T,\epsilon) - \sigma_{3BS}(T,\epsilon) \right] \right] \quad \text{(III.1)}$$

where:

T = The energy of the incident electron in reduced energy units,

ϵ = The energy of the emitted photon in reduced energy units,

f_e is a material-dependent screening parameter, the Elwert factor:

$$f_e(T,\epsilon) = g(T) \; / \; g(T-\epsilon) \quad \text{where} \quad g(T) = \beta(T) \; [\; 1-e^{-2\pi Z/137\beta(T)} \;] \quad ,$$

$c_r(T)$ is an empirical correction factor that is tabulated for each element in DATAPAC, and

$w(T)$ is a weighting parameter:

$$w(T) = \begin{cases} 1.0 & \text{IF } T \geq 50 \\[2mm] \dfrac{(T-8)(T-2)}{2016} - \dfrac{(T-50)(T-2)}{504} & \text{IF } 2.0 < T < 50.0 \\[2mm] 0.0 & \text{IF } T \leq 2.0 \end{cases} \quad ,$$

The microscopic differential cross sections, σ_{3BN}, σ_{3BS}, σ_{3BNb}, and σ_{3CS} are described by Koch and Motz [KOCH].

Note that the Elwert factor becomes infinitely large for radiative events in which the photon emerges with all of the incident electron's energy ($\beta(T-\epsilon) \to 0$.) Hence, the Elwert factor is meaningless in the limit of the high-frequency tail of the bremsstrahlung distribution.

Because bremsstrahlung is primarily due to interactions with the electric field of the nucleus, the bremsstrahlung production cross section for a compound is given by:

$$\sigma^{BP} = \sum_i w_i \sigma_i^{BP}$$

rather than by a form analogous to Eq. II.12. One consequence of this is that when CEPXS constructs the multigroup-Legendre cross sections for a collection of materials, bremsstrahlung transfer matrices must be calculated separately for each unique element in that material collection.

The σ_{3BS} cross section (Born approximation with screening) has the following form:

$$\frac{\sigma_{3BS}(T,\epsilon)}{d\epsilon} = \frac{4C}{\epsilon} \left[\left[1 + \frac{T_s^2}{T^2} \right] \left[\frac{\phi_1(\gamma)}{4} - \frac{\log Z}{3} \right] - \frac{2T_s}{3T} \left[\frac{\phi_2(\gamma)}{4} - \frac{\log Z}{3} \right] \right]$$

$$(III.2)$$

where the screening factors ϕ_1 and ϕ_2 are defined as:

$$\phi_1(\gamma) = 20.867 - 4.409\gamma + 1.156\gamma^2 \qquad \text{IF } \gamma \leq .735 \ ,$$

$$\phi_2(\gamma) = 20.209 - 2.625\gamma - .159\gamma^2 \qquad \text{IF } \gamma \leq .735 \ ,$$

$$\phi_1(\gamma) = 19.83 - 4.184 \log(\gamma + .7) \quad \text{IF } \gamma > .735 \ ,$$

$$\phi_2(\gamma) = \phi_1(\gamma) \quad \text{IF } \gamma > .735 \ ,$$

where:

$$\gamma = \frac{100\ \epsilon}{T\ T_s\ Z^{1/3}}$$

T_s = The kinetic energy of the electron after radiative emission in reduced energy units,

and the coefficient is given by:

$$C = \frac{Z\ (Z+1)\ r_0^2}{137} \quad .$$

Bremsstrahlung production from interaction with the electric field of the atomic electrons is accounted for in CEPXS by using $Z(Z+1)$ in the expression for the coefficient rather than Z^2. (Radiative emission in the field of the atomic electrons is accounted for in a similar way in ITS.)

The σ_{3BN} cross section (Born approximation with no screening) assumes the following form:

$$
\frac{d\sigma_{3BN}(T,\epsilon)}{d\epsilon} = \frac{C\ P_s}{\epsilon\ p}\left\{ \frac{4}{3} - 2TT_s\left(\frac{p_s^2 + p^2}{p_s^2 p^2}\right) + \frac{\chi T_s}{p^3} + \frac{\chi_s T}{p_s^3} + \frac{\chi_s \chi}{p\ p_s} + L\left[\frac{8TT_s}{3pp_s} + \right.\right.
$$

$$
\left.\left. \frac{\epsilon^2(T^2 T_s^2 + p^2 p_s^2)}{p^3 p_s^3} + \frac{\epsilon}{2pp_s}\left(\left[\frac{TT_s + p^2}{p^3}\right]\chi - \left[\frac{TT_s + p_s^2}{p_s^3}\right]\chi_s + \frac{2\epsilon TT_s}{p^2 p_s^2}\right)\right]\right\}
$$

(III.3)

where:

$$p = \text{(the momentum of the incident electron)}/m_e c^2 = [T(T+2)]^{1/2} \quad ,$$

$$p_s = \text{(the momentum of the scattered electron)}/m_e c^2 \quad ,$$

$$\chi = \text{Log} \left(\frac{T + p}{T - p} \right) \quad ,$$

and

$$L = 2 \, \text{Log} \left[\frac{T \, T_s + p \, p_s - 1}{\epsilon} \right]$$

The σ_{3BNb} cross section (Born approximation, no screening, and non-relativistic) has the following form:

$$\frac{d\sigma_{3BNb}(T,\epsilon)}{d\epsilon} = \frac{4C}{\epsilon} \left[1 + \frac{T_s^2}{T^2} - \frac{2 \, T_s}{3 \, T} \right] \left[\text{Log} \left(\frac{2 \, T \, T_s}{\epsilon} \right) - \frac{1}{2} \right] \qquad \text{(III.4)}$$

and the cross section, σ_{3CS}, (Coulomb correction with screening) can be expressed as:

$$\frac{d\sigma_{3CS}}{d\epsilon} = \frac{4C}{\epsilon} \left(\left[1 + \frac{T_s^2}{T^2} \right] \left[\frac{\phi_1(\gamma)}{4} - \frac{\text{Log}(Z)}{3} - f(Z) \right] - \frac{2T_s}{3T} \left[\frac{\phi_2(\gamma)}{4} - \frac{\text{Log}(Z)}{3} - f(Z) \right] \right)$$

$$\text{(III.5)}$$

where:

$$f(Z) = \varsigma^2 \left[\frac{1}{1+\varsigma^2} + .20206 - .0369\varsigma^2 + .0083\varsigma^4 - 0.002\varsigma^6 \right]$$

and $\varsigma = Z/137$.

III.2 CATASTROPHIC RADIATIVE SCATTERING

In CEPXS, catastrophic radiative scattering is modelled by the bremsstrahlung production cross section rewritten as σ^{CB}, a cross section that is differential in the energy of the scattered electron.

Electron slowing down due to soft radiative scattering is modelled by the restricted CSD approximation.

Like the Moller cross section, the bremsstrahlung cross section of Eq. III.1 becomes singular as the energy of the secondary particle produced (the photon) goes to zero. Hence, as for the Moller cross section, some low-energy cutoff must be employed on the integration of the bremsstrahlung cross section over photon energy. However, unlike the Moller cross section, the bremsstrahlung cross section could be applied to all radiative energy transfers [BART]. In CEPXS, the restricted CSD approximation for soft radiative events is used because it is somewhat more efficient (i.e. an accurate solution can be obtained with fewer electron groups.) Hence, energy-loss straggling is implicit only for catastrophic radiative events. Since all radiative events are modelled with a microscopic cross section in ITS, energy loss-straggling is entirely implicit in ITS.

As in ITS, CEPXS assumes that the incident electron does not undergo angular deflection as a result of bremsstrahlung emission. Hence the scattering cross section, σ_{CB}, for catastrophic radiative interactions that is differential in the energy of the scattered electron is:

$$\frac{d\sigma^{CB}}{dT_s d\Omega_s} = \frac{d\sigma^{CB}}{dT_s} \frac{1}{2\pi} \delta(\mu_s - 1.0) \qquad \text{(III.6)}$$

where μ_s is the cosine of the angle of scatter of the electron relative to its initial direction.

The total cross section associated with catastrophic radiative emission is obtained by integrating Eq. III.6 over all photon energies. Because the bremsstrahlung cross section is singular at zero photon energy, this integration must be truncated at a scattered electron energy that corresponds to a non-zero photon energy, ϵ_{cb}. In the high-frequency limit in which the photon energy is comparable to the incident electron's energy, the Elwert factor goes to infinity and the Koch and Motz cross sections go to zero. As suggested by Berger and Seltzer, the bremsstrahlung cross section of Eq. III.1 should not be used when the energy of the bremsstrahlung photon is nearly the same as that of the incident electron. They recommend that some high frequency limit for the bremsstrahlung cross section, based on theory and experiment, be used instead.

Rather than adopting some alternate formulism for the bremsstrahlung cross section in the high-frequency limit, we chose to truncate the integration of the bremsstrahlung cross section in CEPXS at a maximum

photon energy, ϵ_{max}. The maximum photon energy that is allowed in CEPXS
is arbitrarily set to be one keV less than the energy of the incident
electron.

The total cross section associated with catastrophic radiative emission
is:

$$\sigma_t^{CB}(T) = \int_{T-\epsilon_{max}}^{T-\epsilon_{cb}} dT_s \frac{d\sigma^{CB}(T,T_s)}{dT_s} \qquad (III.7)$$

In CEPXS, a catastrophic radiative event is defined to be one in which
an electron down-scatters in energy into non-adjacent energy groups.
For an electron of energy (T) in group (g), the maximum energy that an
electron can have after a catastrophic radiative event is T_{g+2}. Hence,
the lower photon energy cutoff for catastrophic radiative emission is
$\epsilon_{cb} = T - T_{g+2}$.

The total multigroup cross sections for catastrophic radiative emission
are:

$$\sigma_{t,g}^{CB} = \frac{1}{\Delta T_g} \int_{T_{g+1}}^{T_g} dT \int_{T-\epsilon_{max}}^{T_{g+2}} dT_s \frac{d\sigma^{CB}(T,T_s)}{dT_s} \qquad (III.8)$$

The expansion coefficients of the transfer matrices for catastrophic
radiative emission are:

FOR L = 0,1,...LMAX
FOR g' = g+2, g+1, ... G:

$$\sigma_{g \to g',L}^{CB} = \frac{1}{\Delta T_g} \int_{T_{g+1}}^{T_g} dT \int_{T_{g'+1}}^{T_{g'}} dT_s \frac{d\sigma^{CB}}{dT_s} \qquad (III.9)$$

The effective absorption cross sections due to catastrophic radiative
emission are:

$$\sigma_{a,g}^{CB} = \sigma_{t,g}^{CB} - \sum_{g' > g} \sigma_{g \to g',0}^{CB} \qquad (III.10)$$

The effective energy deposition cross sections for scattering by

catastrophic radiative emission are:

$$\sigma^{CB}_{E,g} = \sigma^{CB}_{t,g} \, E^m_g - \sum_{g' > g} \sigma^{CB}_{g \to g',0} \, E^m_{g'} \qquad \text{(III.11)}$$

while the charge deposition cross sections for catastrophic radiative emission are:

$$\sigma^{CB}_{C,g} = \sigma^{CB}_{a,g} \qquad \text{(III.12)}$$

III.3 BREMSSTRAHLUNG PRODUCTION

In CEPXS, the cross section for bremsstrahlung photon production is separated into a cross section that is differential in the energy of the photon and into a normalized differential angular distribution:

$$\frac{d\sigma^{BP}}{d\epsilon \, d\Omega} = \frac{d\sigma^{BP}}{d\epsilon} \, \frac{dW(\mu,T)}{d\Omega} \qquad \text{(III.13)}$$

where μ is the cosine of the emitted photon relative to the direction of the electron prior to radiative emission.

The Sommerfield angular distribution of bremsstrahlung photons [SANDYL] is used in CEPXS:

$$\frac{dW(\mu,T)}{d\Omega} = \frac{1}{2\pi} \, \frac{dW(\mu,T)}{d\mu} = \frac{1 - \beta^2}{4\pi \, (1-\beta\mu)^2} \qquad \text{(III.14)}$$

As the energy of the incident electron increases $(\beta \to 1)$, the bremsstrahlung angular distribution becomes increasingly forward peaked.

In order for electrons in group (g) to produce photons in group (f), the maximum energy for an electron in the group (T_g) must exceed the lower energy boundary of that photon group, ϵ_{f+1}. The expansion coefficients of the transfer matrices for bremsstrahlung emission are:

FOR L = 0,1,...LMAX:

FOR PHOTON GROUPS f = 1, 2, ... F:

$$\sigma^{PB}_{g \to f,L} = \frac{1}{\Delta T_g} \int_{T_{g+1}}^{T_g} dT \int_{\epsilon_{f+1}}^{Min \left[\epsilon_f , \epsilon_{max} \right]} d\epsilon \ H[\Delta\epsilon] \ W_L(T) \ \frac{d\sigma^{BP}(T,\epsilon)}{d\epsilon}$$

where the argument of the step function is:

$$\Delta\epsilon = Min \left[\epsilon_f , \epsilon_{max} \right] - \epsilon_{f+1}$$

Most bremsstrahlung photons are correlated in energy with electrons that are scattered in catastrophic radiative events. However, if ϵ_{cb} exceeds ϵ_{F+1}, those photons with energy less than ϵ_{cb} are associated with soft radiative emission. As was the case for soft collisions, soft radiative energy losses are not correlated in energy with the production of secondary particles. The energy domain that the user defines for the calculation can also impact the extent of the energy correlation for catastrophic events. For instance, if ϵ_{cb} is less than the cutoff energy, electrons can lose energy in a catastrophic radiative event without the appearance of bremsstrahlung photons in any photon energy group.

The moments of the normalized angular distribution for the bremsstrahlung photons:

$$W_L(T) = 2\pi \int_{-1}^{1} P_L(\mu) \ W(T,\mu) \ d\mu \quad ,$$

are evaluated in recursive fashion in CEPXS:

$$W_0(T) = 1.0$$

$$W_1(T) = \frac{2\beta + (1-\beta^2) \ Log \left[\frac{1 - \beta}{1 + \beta} \right]}{2\beta^2}$$

$$W_L(T) = \frac{(2L-1)W_{L-1} - (L)\beta W_{L-2}}{(L-1)\beta}$$

Note that as the energy of the incident electron increases ($\beta \to 1$), the Legendre moments of the bremsstrahlung angular distribution become increasingly like those of a delta function. For low-energy electrons, the bremsstrahlung distribution is close to being isotropic and it is

sufficient to calculate only a few moments of the distribution. In CEPXS, when the expansion given by Eq. III.16 yields a ratio of W_L/W_O less than .0001, the higher-order Legendre moments (L+1,L+2,...LMAX) are not evaluated but are set equal to zero.

In CEPXS, the calculation of the transfer matrix for bremsstrahlung production is simplified by the assumption that all the electrons in a group emit bremsstrahlung with the same angular distribution:

$$W_L(T) \simeq W_L(T_g^m)$$

The effective energy cross sections due to bremsstrahlung production are:

$$\sigma_{E,g}^{BP} = -\sum_f \sigma_{g \to f,0}^{BP} \; E_f^m \qquad (III.17)$$

while the secondary production cross sections due to bremsstrahlung production are:

$$\sigma_{S,g}^{BP} = \sum_f \sigma_{g \to f,0}^{BP} \qquad (III.18)$$

The production of bremsstrahlung radiation does not contribute to total, absorption, or charge deposition reactions.

III.4 SOFT RADIATIVE SCATTERING

The restricted CSD approximation is used to characterize soft radiative energy losses. As was the case for soft collisions, soft radiative emission results in the down-scatter of an electron into the adjacent energy group. Energy-loss straggling is not associated with soft radiative emission.

Soft radiative events are represented in CEPXS by "pseudo" cross sections that are similar in form to those in Section II.4. These cross sections represent the differenced form of the restricted CSD operator. Multigroup-Legendre matrices for electron-to-electron transfers due to soft radiative events can be constructed from these CSD cross sections. The expansion coefficients of the matrices associated with the first-order differenced form of the restricted CSD operator [MOR2] are:

FOR L = 0,1,...LMAX:

FOR g = 1,2,...G-1:

$$\sigma^{SB}_{g \to g', L} = \frac{R^B(E^m_g)}{E^m_g - E^m_{g'}} \quad \text{IF } g' = g+1 \tag{III.19}$$

where R^B is the restricted radiative stopping power, and

E^m_g is the midpoint energy of group g.

In the CSD approximation, the electron slows down without angular deflection. This delta function scattering is represented by a truncated Legendre expansion:

FOR L = 0,1,...LMAX:

FOR g = 1,2,...G-1:

$$\sigma^{SB}_{g \to g', L} = \sigma^{SB}_{g \to g', 0} \quad \text{IF } L \leq \text{LMAX} \tag{III.20}$$

The expansion coefficients of the Lth-order transfer matrix associated with the diamond differenced form of the CSD operator [MOR3] are:

$$\sigma^{SB}_{g \to g', L} = \frac{(-1)^{g'-g+1}}{\Delta E_g} 2 \left[R^B(E_{g'}) + R^B(E_{g'+1}) \right] \quad \text{IF } G > g' > g \tag{III.21}$$

$$= \frac{(-1)^{G-g+1}}{\Delta E_g} 2 \left[R^B(E_G) + S^B(E_{G+1}) \right] \quad \text{FOR } g' = G$$

$$= 0 \quad \text{OTHERWISE}$$

The effective absorption cross sections due to soft radiative emission are:

$$1^{st} \text{ order} \quad \begin{cases} \sigma^{SB}_{a,g} = 0 & \text{IF } g = 1, 2, \ldots G-1 \\ \\ = \dfrac{R^B \left(E^m_g \right)}{E^m_g - E_u} & \text{IF } g = G \end{cases} \tag{III.22}$$

$$2^{\text{nd}} \text{ order} \quad \left\{ \quad \sigma_{a,g}^{SB} = \frac{(-1)^{G-g} 2 S^{B}(E_{G+1})}{\Delta E_{g}} \quad \text{FOR } g = 1,2,\ldots G \right.$$

where E_u is the midpoint energy of the fictitious energy group constructed below the cutoff energy, T_{G+1}.

The total cross sections for soft radiative emission are:

$$1^{\text{st}} \text{ order} \quad \left\{ \quad \sigma_{t,g}^{SB} = \sigma_{a,g}^{SB} + \sigma_{g \to g+1,0}^{SB} \right.$$

$$2^{\text{nd}} \text{ order} \quad \left\{ \quad \sigma_{t,g}^{SB} = \sigma_{a,g}^{SB} + \sum_{g' > g} \sigma_{g \to g',0}^{SB} \right.$$

(III.23)

The energy deposition cross sections due to soft radiative emission are:

$$1^{\text{st}} \text{ order} \quad \left\{ \begin{array}{ll} \sigma_{E,g}^{SB} = 0 & \text{IF } g \leq G \\[2mm] = \sigma_{a,g}^{SB} E_g^m & \text{IF } g = G \end{array} \right.$$

(III.24)

$$2^{\text{nd}} \text{ order} \quad \left\{ \quad \sigma_{E,g}^{SB} = \sigma_{t,g}^{SB} E_g^m - \sum_{g' > g} \sigma_{g \to g',0}^{SB} E_{g'}^m \right.$$

while the charge deposition cross sections for soft radiative emission are:

$$\sigma_{C,g}^{SB} = \sigma_{a,g}^{SB}$$

(III.25)

III.5 THE RESTRICTED RADIATIVE STOPPING POWER

In order to evaluate the CSD cross sections for soft radiative emission, the restricted radiative stopping power, R^B, must be calculated. For the cross sections that correspond to a first-order differenced form of the restricted CSD operator, the restricted radiative stopping power must be evaluated at the midpoint energies of all electron groups except the last. The restricted radiative stopping power is defined as that portion of the total radiative stopping power that is not associated with catastrophic energy loss:

FOR L = 0,1,...LMAX: (III.26)
FOR g = 1,2,...G-1:

$$R^B(E_g^m) = S^B(E_g^m) - \frac{m_e^2 c}{\Delta T_g} \int_{T_{g+1}}^{T_g} dT \int_{T-\epsilon_{max}}^{T_{g+2}} dT_s \ (T-T_s) \ \frac{d\sigma^{CB}(T,T_s)}{dT_s}$$

where $S^B(E)$ is the total radiative stopping power (in units of MeV-cm^2/g).

As shown in Fig. 6, the magnitude of the stopping power associated with catastrophic radiative loss is comparable to the total radiative stopping power even when few electron groups are used. With 160 groups, the stopping power that is due to catastrophic radiative energy losses is nearly identical to the total radiative stopping power. This is quite different from the case with collisional scattering (cf. Fig. 1.) The large share of the radiative stopping power due to catastrophic radiative energy losses is consistent with our earlier assertion in Section 3.2 that the single-event bremsstrahlung cross section is more amenable to a multigroup representation than is the single-event cross section for collisions.

In order to evaluate the cross sections that represent the second-order differenced form of the restricted CSD operator, the restricted radiative stopping power must be evaluated at all electron group boundaries except the upper boundary, E_1, and the lower boundary, E_{G+1}. As was the case with the restricted collisional stopping power, two different interpretations are possible for the restricted radiative stopping power at a group boundary energy. If E_g is considered to be the upper boundary of group, then the restricted radiative stopping power is:

FOR g = 2,3, ... G-1:

$$R_U^B(E_g) = S^B(E_g) - m_e c^2 \int_{T_g-\epsilon_{max}}^{T_{g+2}} dT_s \ (T_g-T_s) \ \frac{d\sigma^{CB}(T_g,T_s)}{dT_s} \qquad (III.27)$$

and:

$$R_U^B(E_G) = 0$$

On the other hand, if E_g is considered to be the lower boundary of a group, the restricted radiative stopping power is:

FOR $g = 2,3, \ldots G$:

$$R_L^B(E_g) = S^B(E_g) - m_e c^2 \int_{T_g - \epsilon_{max}}^{T_{g+1}} dT_s \; (T_g - T_s) \; \frac{d\sigma^{CB}(T_g, T_s)}{dT_s} \qquad \text{(III.28)}$$

To avoid ambiguity, the restricted radiative stopping power at a group boundary is defined to be the average of the previous two formulations:

FOR $L = 0,1,\ldots$LMAX:

FOR $g = 2,3,\ldots$G:

$$R^B(E_g) = \frac{1}{2} \left[R_U^B(E_g) + R_L^B(E_g) \right] \qquad \text{(III.29)}$$

IV. ELASTIC ELECTRON SCATTERING

Both the CEPXS and ITS codes use the same cross section for the elastic scattering of electrons in the nuclear field of an atom. For electrons with relativistic kinetic energies (> 256 keV), both codes use the Mott cross section with Moliere screening. At non-relativistic energies, the elastic scattering cross section data developed by Riley et. al. [RILEY] is used instead.

In ITS, the nuclear elastic scattering cross sections are modified to account for inelastic deflections. This is accomplished by multiplying the nuclear elastic scattering cross section at the angles $\theta \leq \theta_{max}$ by the ratio $(Z+1)/Z$. The angle θ_{max} is the maximum angle of deflection of an electron by an inelastic collision (see Chapter II.2.) This is not done in CEPXS since angular deflections associated with catastrophic collisions are correlated with energy loss through the Moller cross section.

In ITS, the elastic-scattering cross sections appear in the context of a condensed-history model, the Goudsmit-Saunderson theory of multiple-scattering. In CEPXS, elastic scattering is based on a microscopic cross section. However, this highly forward-peaked elastic-scattering cross section is modified by the extended transport correction. This approximation makes the elastic-scattering cross section amenable to a low-order Legendre expansion.

IV.1 THE MOTT CROSS SECTION WITH MOLIERE SCREENING

For an element, the macroscopic Mott cross section with Moliere screening in units of cm^2/g is: [BERG2], [ZERBY]

$$\frac{d\sigma^E(T,\theta)}{d\Omega} = \frac{C(T)}{\left[1-\cos\theta+2\eta(T)\right]^2} \left[1 + \frac{\pi}{\sqrt{2}}\frac{Z}{137}\beta\chi(T)\left[1-\cos\theta+2\eta(T)\right]^{1/2} + h(\theta,T)\right]$$

$$(IV.1)$$

where:

T = The kinetic energy of the electron in reduced energy units,

$$C(T) = \frac{2\pi r_0^2 N_A Z^2}{A} \quad \frac{(T+1)^2}{T^2(T+2)^2} \quad ,$$

$$h(\theta,T) = D(\theta,T) - 1 - \frac{\pi}{\sqrt{2}}\frac{Z}{137}\beta \chi(T) \left[1 - \cos\theta + 2\eta(T)\right]^{1/2} ,$$

$$\eta(T) = \frac{.25\ Z^{2/3} \left[1.13 + 3.76 \left(\frac{Z}{137} \right)^2 (T+1)^2\ T^{-1}\ (T+2)^{-1} \right]}{(.885 * 137)^2\ T\ (T+2)} ,$$

The function, $\chi(T)$ is tabulated at discrete energies on the DATAPAC data tape for electrons [ETRAN]. The function, $D(\theta,T)$, represents the ratio of the Mott cross section to the Rutherford cross section at a given energy and angle of scatter. This function is also tabulated on the DATAPAC data tape at discrete energies and at the discrete angles: $\theta = 0, 45°, 90°, 135°, 180°$.

The Lth-order transfer matrix for elastic scattering consists only of diagonal terms:

FOR L = 0,1,...LMAX:

$$\sigma^E_{L,g\to g'} = \frac{\int_{T_{g+1}}^{T_g} W_E(T)\,dT \int d\Omega\ \frac{d\sigma^E(T,\theta)}{d\Omega}\ P_L(\cos\theta)}{\int_{T_{g+1}}^{T_g} W_E(T)\ dT}\ \delta_{gg'} \qquad (IV.2)$$

where $W_E(T)$ is the multigroup weight function for elastic scattering and $\delta_{gg'}$ is the Kronecker delta. In CEPXS, a weight function that is consistent with elastic scattering is selected:

$$W_E(T) = \delta(T-T^m_g) \qquad (IV.3)$$

where T^m_g is the midpoint energy of the group.

Hence, the expansion coefficients of the transfer matrices associated with elastic scattering are:

$$\sigma^E_{L,g\to g'} = \sigma^E_L(T^m_g)\ \delta_{gg'} \qquad (IV.4)$$

where:

$$\sigma^E_L(T) = \int d\Omega\ \frac{d\sigma^E(T,\theta)}{d\Omega}\ P_L(\cos\theta) \qquad (IV.5)$$

The total cross sections associated with elastic scattering are:

$$\sigma^E_{t,g} = \sigma^E_{0,g \rightarrow g} \qquad \text{(IV.6)}$$

Instead of evaluating these moments by quadrature, CEPXS uses a semi-analytical approach devised by Berger [BERG2]. In this approach, the moments of the Goudsmit-Saunderson (G-S) distribution, which are directly related to the moments of the elastic scattering cross section, are evaluated. The G-S moments are:

$$
\begin{aligned}
G_L(T) &= 2\pi \int_{-1}^{1} d\mu \; \frac{d\sigma^E(T,\theta)}{d\Omega} \left[1 - P_L(\cos\theta) \right] \\
&= \sigma^E_0(T) - \sigma^E_L(T)
\end{aligned}
\qquad \text{(IV.7)}
$$

The G-S moments can be expressed in terms of the special functions devised by Spencer [SPENCE]:

$$p(m,L) = \int_{-1}^{1} (1-x+2\eta)^m \left[1 - P_L(x) \right] dx \qquad \text{(IV.8)}$$

if the function, $h(\theta,T)$, by:

$$h(\theta,T) \simeq \sum_{j=1}^{5} h_j \left[1-\cos\theta+2\eta(T) \right]^{j-1} \qquad \text{(IV.9)}$$

The coefficients in this expansion, h_j, are numerically calculated by demanding that the expansion be exact for the five angles at which the function, $D(\theta,T)$, is tabulated in the DATAPAC data tape.

With this approximation, the G-S moments for the Mott cross section with Moliere screening can be expressed in the analytical form as:

$$G_L(T) = 2\pi C(T) \left[p(-2,L) + \frac{\pi Z \beta}{\sqrt{2} \; 137} \chi(T) \; p(-3/2,L) + \sum_{j=1}^{5} h_j \; p(j-1-2,L) \right]$$

$$\text{(IV.10)}$$

The recursion relations needed to construct the functions, $p(m,L)$, for m = -3/2, -2, -1, 0, 1, 2 and arbitrarily high Legendre order are

contained in a reference by Berger [BERG2].

IV.2 THE RILEY CROSS SECTION

The Mott cross section for elastic scattering is accurate only for relativistic electrons (E > 256 keV). For the elastic scattering of electrons, with lower energies (down to 1.0 keV), both ITS and CEPXS use the cross section derived by Riley et. al. [RILEY].

This cross section can be fitted by 12 energy-dependent parameters (A_m, B, C_n) in the following fashion:

$$\frac{d\sigma^E(T,\theta)}{d\Omega} = D \left[\sum_{m=1}^{4} A_m(T) \left(1- \mu + 2B(T)\right)^{-m} + \sum_{n=0}^{6} C_n(T) \; P_n(\mu) \right] \qquad (IV.11)$$

The G-S moments with the Riley cross section are:

$$G_L(T) = 2\pi D \left[\sum_{m=1}^{4} A_m(T) \; p^*(-m,L) + C_0(T) - C_L(T) \right] \qquad (IV.12)$$

where δ_{LO} is the Kronecker delta and the Spencer functions, $p^*(m,L)$, are defined as:

$$p^*(m,L) = \int_{-1}^{1} (1-x+2B)^m \left[1 - P_L(x) \right] dx \qquad (IV.13)$$

CEPXS obtains the parameters needed to construct the Riley elastic-scattering cross section from the electron data tape.

IV.3 THE EXTENDED TRANSPORT CORRECTION

Since the elastic-scattering cross section for electrons is highly forward peaked, an accurate Legendre expansion of this cross section would require an expansion to very high order. A lower-order expansion is feasible if the extended transport correction is applied to the elastic scattering cross section. In this approach, the elastic scattering cross section is "corrected" by the removal of a delta-function component. This approach has been studied for both neutrons [BELL] and electrons [MOR1]. In CEPXS, the extended transport correction is applied to both the Mott and the Riley cross sections.

In the extended transport correction, the highly forward-peaked elastic scattering cross section is approximated by a corrected cross section, σ^*, and a delta function component:

$$\sigma^E(\mu) \simeq \sigma^*(\mu) + \frac{C}{2\pi} \delta(\mu-1) \qquad (\text{IV}.14)$$

where C is an arbitrary constant. (The energy dependence of the cross sections is suppressed in this discussion.) The corrected cross section can be represented by a finite Legendre expansion:

$$\sigma^*(\mu) = \sum_{L=0}^{LMAX} \frac{2L+1}{4\pi} \sigma_L^* \ P_L(\mu) \qquad (\text{IV}.15)$$

If we require that decomposition of the elastic cross section into a corrected cross section and a delta function to be accurate to Legendre order, LMAX, then the Legendre moments of the corrected cross sections differ from those of the elastic-scattering cross section by a constant:

$$\sigma_L^* = \sigma_L^E - C \qquad (\text{IV}.16)$$

for L = 0, 1, ... LMAX.

In CEPXS, the terms of the transfer matrix for the elastic-scattering cross sections are constructed using these moments:

$$\sigma_{L,g \rightarrow g'}^E = \sigma_L^*(T_g^m) \ \delta_{gg'} \qquad (\text{IV}.17)$$

It is possible for the corrected cross section to be negative at certain values of μ. While such a cross section can be used in discrete ordinates codes, they are not acceptable for use in multigroup Monte Carlo codes which sample over μ.

A unique corrected cross section does not exist. In order to specify a particular σ^*, we must specify C. One way of doing so is to require that:

$$\sigma_{LMAX}^* = 0 \qquad (\text{IV}.18)$$

This is the approach used in CEPXS. With this requirement, the moments of the corrected cross section become:

$$\sigma_L^* = \sigma_L^E - \sigma_{LMAX}^E$$

$$= G_{LMAX} - G_L \qquad \text{(IV.19)}$$

V. IMPACT IONIZATION AND RELAXATION PRODUCTION

In both the CEPXS and ITS codes, impact ionizations are not correlated with inelastic collisions. A special impact ionization cross section is used in both codes solely to determine the production of relaxation radiation (Auger electrons and fluorescence photons.) The energy of a relaxation particle is less than or equal to the binding energy of the shell that is ionized. Since particles are not tracked below the cutoff energy in either CEPXS or ITS, ionization events in shells with energy less than the cutoff energy are not considered. The minimum cutoff energy allowed by either code is 1 keV. The binding energies of electrons in the K,L1,L2,L3,M, and N shells exceed 1 keV for elements with Z greater than 10, 27, 29, 29, 51, and 84 respectively. In CEPXS, the binding energy of the N shell for elements with Z > 84 is taken to be identically zero.

V.1   THE IMPACT IONIZATION CROSS SECTION

When the NO-PCODE option is selected by a user, CEPXS restricts impact ionization to the K-shell. The Kolbenstvedt [KOLBEN] cross section for impact ionization of the K-shell is used. The macroscopic form of this cross section for a single element is, in units of cm^2/g:

$$\sigma^{I,1}(T) = \frac{8\pi r_0^2 N_A}{3 A \phi_1 \beta^2} \left[.42\ A(T) + 1.5\ B(T) \right] \qquad IF\ T \geq \phi_1$$

$$= 0 \quad IF\ T < \phi_1 \qquad ,$$

where:

$$A(T) = Log\left[\frac{1.19 * (T^2+2T)}{\phi_1} - \beta^2 \right] \quad ,$$

$$B(T) = \left[1 - \frac{\phi_1}{T} \left[1 - \frac{1}{2} \frac{T^2}{(T+1)^2} + \frac{2T+1}{(T+1)^2} Log\left(\frac{T}{\phi_1} \right) \right] \right]$$

(V.1)

ϕ_1 = The K-shell binding energy in reduced energy units.

The numeral in the superscript of the above cross section is the index of the shell where ionization occurs. The convention regarding shell indices that we will follow in this report is that the higher the index, the lower is the binding energy of the associated shell. Thus, an index

of unity is used in Eq. V.1 to indicate that ionization occurs in the K shell.

By default (without the NO-PCODE option), CEPXS employs the impact ionization cross sections developed by Gryzinski [GRYZ]. The microscopic form of the Gryzinski cross section for the impact ionization of an electron in the i-th shell is, in units of cm^2:

$$\xi^{I,i}(T) = \frac{\pi r_0^2}{\phi_i^2} f_v \left\{ 1 + \frac{2}{3} \left[1 - \frac{\phi_i}{2T} \right] Log\left[2.7 + \left(\frac{T}{\phi_i} - 1 \right)^{1/2} \right] \right\} \left(1 - \frac{\phi_i}{T} \right)^{3/2}$$

$$IF \ T \geq \phi_i$$

$$= 0 \ \ IF \ T < \phi_i \quad , \tag{V.2}$$

where: i = Shell index (i = 1,2,3,4,5 : K,L1,L2,L3,"average" M),

$$f_v = \frac{\beta_i^2}{\beta^2} \left[\frac{\beta^2}{\beta^2 + \beta_i^2 - \beta^2 \beta_i^2} \right]^{3/2} \quad ,$$

$$\beta_i^2 = \frac{\phi_i (\phi_i + 2)}{(\phi_i + 1)^2} \quad ,$$

and

ϕ_i = The binding energy of the ith shell in reduced energy units.

The macroscopic form of the Gryzinski cross section for an element is:

$$\sigma^{I,i} = \frac{N_A \ g_i \ \xi^{I,i}}{A} \tag{V.3}$$

where g_i is the number of electrons in a complete shell. For instance, g_i is 2,2,2,4,18 for the K,L1,L2,L3, and M shells, respectively. While the outer shells of most atoms are not complete, there is no need to make g_i dependent on the atomic number in high-energy (above one keV) codes such as CEPXS and ITS. This is because the binding energies of the outermost shell in all atoms is less than the minimum energy allowed by the codes. Hence, ionization in the non-complete outermost shell is irrelevant.

V.2 RELAXATION PRODUCTION

The impact ionization cross section is associated in CEPXS with the production of relaxation radiation. Relaxation radiation consists of Auger electrons and fluorescence photons. These are produced in a cascade of shell transitions induced by the initial vacancy. The energy of a relaxation particle is equal to the difference between the binding energies of the shells involved in a transition.

The impact ionization cross sections of the i-th shell are:

$$
\sigma_g^{I,i} = \frac{\displaystyle\int_{T_{g+1}}^{T_g} dT\ \sigma^{I,i}(T)}{\Delta T_g} \tag{V.4}
$$

Since the impact ionization cross section is solely used to determine the production of relaxation radiation, impact ionization does not contribute to the total reaction rate.

The expansion coefficients of the transfer matrix associated with the production of electron relaxation radiation following impact ionization are:

FOR g = 0,1,...G:

$$
\sigma_{g \rightarrow g',0}^{IE,i} = \sum_{i=1}^{5} \sum_{j=1}^{28} \eta_{ij}^{e}\ \delta_{g'g_j}\ \sigma_g^{I,i}\ , \tag{V.5}
$$

where: i = The index of the ionized shell,

j = The index of the line radiation,

η_{ij}^{e} = The relaxation efficiency that the jth Auger electron is produced following the ionization of the ith shell.

g_j = The electron group that contains the energy of the jth Auger electron.

Since Auger emission is isotropic, only the lowest Legendre-order transfer matrix is shown in Eq. V.5. The higher-order transfer matrices for Auger (and fluorescence) production contain terms that are identically zero.

There are twenty-eight different transitions in the various relaxation cascades that can follow an ionization event. The line radiations associated with each of these transitions are identified in the Chapter VI. The relaxation efficiencies for Auger and fluorescence emission are also discussed in the next chapter.

The transfer matrix associated with fluorescence production resulting from impact ionization consists of the following terms:

FOR g = 1,2,...G:

$$\sigma^{IF}_{g \to f, 0} = \sum_{i=1}^{5} \sum_{j=1}^{28} \eta^{f}_{ij} \, \delta_{ff_j} \, \sigma^{I,i}_{g} \quad , \tag{V.6}$$

where:

η^{f}_{ij} = The relaxation efficiency that the jth fluorescence photon is produced following the ionization of the ith shell,

f_j = The photon group that contains the energy of the jth fluorescence photon.

The effective energy deposition cross sections associated with the production of relaxation radiation by impact ionization are:

$$\sigma^{I}_{E,g} = - \sum_{g'} \sigma^{IE}_{g \to g', 0} \, E^{m}_{g'} - \sum_{f} \sigma^{IF}_{g \to f, 0} \, E^{m}_{f} \tag{V.7}$$

Note that these cross sections are expressed in terms of the midpoint energies rather than line radiation energies, as is consistent with the definition of the effective energy deposition cross section in Eq. I.33.

The charge deposition cross sections associated with the production of relaxation radiation by impact ionization are:

$$\sigma^{I}_{C,g} = - \sum_{g'} \sigma^{IE}_{g \to g', 0} \tag{V.8}$$

while the secondary production cross sections associated with the production of relaxation radiation by impact ionization are:

$$\sigma_{S,g}^{I} = \sum_{g'} \sigma_{g \to g',0}^{IE} + \sum_{f} \sigma_{g \to f,0}^{IF} \qquad (V.9)$$

VI. THE RELAXATION CASCADE

After an atomic shell is ionized, whether by impact ionization or photoelectric ionization, a cascade of relaxation radiation will be produced. An atomic transition is induced by the vacancy created by the initial ionization event. In the subsequent relaxation cascade, these transitions induce vacancies in other shells which lead to the emission of additional line radiation. The relaxation cascade ceases when a transition produces a vacancy in the outermost shell of the atom.

VI.1 THE NO-PCODE OPTION

With the NO-PCODE option, ionization in CEPXS is restricted to the K-shell. Moreover, this option invokes a simple model of the relaxation cascade with only two possible branches. In one branch, a single Auger electron is emitted while in the other, only a single fluorescence photon is emitted. This simplified relaxation cascade is sketched below:

$$
\begin{array}{ccc}
 & K & \\
F \ (K{:}F) \ \diagup & & \diagdown \ A \ \ 1{-}(K{:}F) \\
X & & X
\end{array}
\qquad\qquad (VI.1)
$$
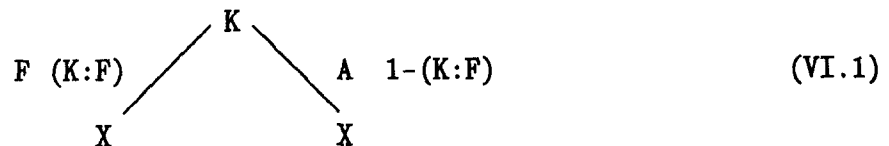
where:

K   denotes a vacancy in the K-shell

X   denotes a vacancy in the outermost shell of the atom

A   denotes a transition that produces an Auger electron

F   denotes a transition that produces a fluorescence photon

(K:F)   denotes the probability that a fluorescence transition from the K-shell occurs

$$= \eta_{11}^{f} \ \text{(cf. the fluorescence efficiency in Eq. V.6)}$$

1-(K:F)   denotes the probability that an Auger transition from the K-shell occurs

$$= \eta_{11}^{e} \ \text{(cf. the Auger efficiency in Eq. V.5)}$$

The K-shell fluorescence efficiency [BURHOP] of an element can be expressed as a function of the atomic number by:

$$(K:F) = -A + BZ - CZ^3 \quad , \quad\quad\quad (VI.2)$$

where:

A = .064
B = .034
C = .00103 .

The coefficients in the formula for the fluorescence efficiency have been experimentally determined [HAGE].

In this simplified cascade, both the fluorescence photon and the Auger electron are emitted with the same energy. This line energy is slightly less than the K-shell binding energy and represents an "average" of the energies that these particles would acquire in a real relaxation cascade. The line radiation energies that are used in CEPXS with the NO-PCODE option are identical to those employed in the non-P-code members of ITS.

VI. THE PCODE CASCADE

More complex relaxation cascades are used by CEPXS if the NO-PCODE option is not invoked. These cascades are essentially equivalent to that in the PCODES of ITS. The only difference is that, in CEPXS, the binding energy of the N-shell is assumed to be zero for all elements. In ITS, only the N-shell binding energies for elements with Z less than 85 are assumed to be zero.

The complex relaxation cascades of both CEPXS and ITS were originally developed for the SANDYL Monte Carlo code [SANDYL]. The radiation cascade that follows M-shell ionization is shown in Fig. 7(a). The radiation cascades that follows ionization of the L1, L2, and L3 shells are partially shown in Fig. 7(b). The full relaxation cascade from these shells is obtained by a combination of Figs. 7(a,b). The radiation cascade that follows ionization of the K shell is partially shown in Fig. 7(c). Since the K-shell relaxation cascade induces ionizations in the L1, L2, L3 and M shells, the complete K-shell ionization cascade is obtained by a combination of Figs. 7(a,b,c).

CEPXS obtains from the electron data tape the shell binding energies,

ϕ_i, that are needed to calculate the line radiation energies. Also obtained from this data tape is the information necessary to calculate the relaxation efficiencies for Auger production, η^e and fluorescence production, η^f. In ITS, such data resides in an array of relaxation quantities [HALB]. In CEPXS, an identical array is used to store similar information. The parameters that are stored in this array are referred to as relaxation quantities. A relaxation quantity is denoted in this report by a bracketed integer which indicates the array index in which this information is stored. For instance, the shell binding energies for the K,L1,L2,L3 and M shells are stored in the relaxation quantity array at indices [2], [4], [6], [7], [8], respectively.

The relaxation efficiencies are calculated using probability parameters stored in the relaxation quantity array. These parameters are the conditional probabilities for portions of the relaxation cascade. For instance, the relaxation quantity, [5], is a probability parameter that denotes the probability that a Auger KLL transition has produced vacancies in the L2 and L3 shells. This probability parameter is denoted in the tables below by (KLL:L2+L3|A:KLL|K:A). Similar notation is used to describe the other parameters.

Table VI.1 Line Radiation from K-Shell Partial Cascade, Fig. 7(c)

INDEX		η^e_{1j}	η^f_{1j}
j	ENERGY		
1	ϕ_K	(1-[1]) (1-[11]-[12]) (.045)	[1] (1-[49]-[50]-[51])
2	$\phi_K - \phi_M$	(1-[1]) (1-[11]-[12]) (.045)	[1] [51]
3	$\phi_K - \phi_M - \phi_M$	(1-[1]) (1-[11]-[12]) (.91)	-
4	$\phi_K - \phi_{L3}$	(1-[1]) [12] (1-[63]) (1-[61]-[62])	[1] [46]
5	$\phi_K - \phi_{L2}$	(1-[1]) [12] (1-[63]) [62]	[1] [50]
6	$\phi_K - \phi_{L1}$	(1-[1]) [12] (1-[63]) [61]	-
7	$\phi_K - \phi_{L3} - \phi_M$	(1-[1]) [12] [63] (1-[61]-[59])	-
8	$\phi_K - \phi_{L2} - \phi_M$	(1-[1]) [12] [63] [60]	-
9	$\phi_K - \phi_{L1} - \phi_M$	(1-[1]) [12] [63] [59]	-

10 $\phi_K - \phi_{L3} - \phi_{L1}$ (1-[1]) [58] [11]   –

11 $\phi_K - \phi_{L1} - \phi_{L3}$ (1-[1]) [57] [11]   –

12 $\phi_K - \phi_{L2} - \phi_{L2}$ (1-[1]) [11] (1-[5]-[55]-[56]-[57]-[58])   –

13 $\phi_K - \phi_{L2} - \phi_{L3}$ (1-[1]) [5] [11]   –

14 $\phi_K - \phi_{L1} - \phi_{L2}$ (1-[1]) [56] [11]   –

15 $\phi_K - \phi_{L1} - \phi_{L1}$ (1-[1]) [55] [11]   –

where:

[1] = (K:F)   [56] = (KLL:L1+L2|A:KLL|K:A)

[5] = (KLL:L2+L3|A:KLL|K:A)   [57] = (KLL:L1+L3|A:KLL|K:A)

[11] = (A:KLL|K:A)   [58] = (KLL:L3+L3|A:KLL|K:A)

[12] = (A:KLX|K:A)   [59] = (KLM:L1+M|KLX:KLM|A:KLX|K:A)

[49] = (F:L3|K:F)   [60] = (KLM:L2+M|KLX:KLM|A:KLX|K:A)

[50] = (F:L2|K:F)   [61] = (KLN:L1+N|KLX:KLN|A:KLX|K:A)

[51] = (F:M|K:F)   [62] = (KLN:L2+N|KLX:KLN|A:KLX|K:A)

[55] = (KLL:L1+L1|A:KLL|K:A)   [63] = (KLX:KLM|A:KLX|K:A)

Table VI.2 Line Radiation from L1-Shell Partial Cascade, Fig. 7(b)

INDEX j	ENERGY	η^e_{2j}	η^f_{2j}
16	ϕ_{L1}	(1-[21]-[48]-[47]) (1-[39]-[33])	[21] (1-[24])
17	$\phi_{L1}-\phi_M$	(1-[21]-[48]-[47]) [39]	[21] [24]
18	$\phi_{L1}-\phi_{L2}$	[48]	–
19	$\phi_{L1}-\phi_{L3}$	[47]	–
20	$\phi_{L1}-\phi_M-\phi_M$	(1-[21]-[48]-[47]) [33]	–

where:

[21] = (L1:F)   [39] = (A:M+N|L1:A)

[24] = (F:M|L1:F)   [47] = (L1:L3)

[33] = (A:M+M|L1:A)   [48] = (L1:L2)

Table VI.3 Line Radiation from L2-Shell Partial Cascade, Fig. 7(b)

INDEX j	ENERGY	η^e_{3j}	η^f_{3j}
21	ϕ_{L2}	(1-[20]-[46]) (1-[32]-38])	[20] (1-[23])
22	$\phi_{L2}-\phi_M$	(1-[20]-[46]) [38]	[20] [23]
23	$\phi_{L2}-\phi_{L3}$	[46]	–
24	$\phi_{L2}-\phi_M-\phi_M$	(1-[20]-[46]) [32]	–

where:

[20] = (L2:F)   [38] = (A:M+N|L2:A)

[22] = (F:M|L2:F)   [46] = (L2:L3)

[32] = (A:M+M|L2:A)

Table VI.4 Line Radiation from L3-Shell Partial Cascade, Fig. 7(b)

INDEX j	ENERGY	η^e_{4j}	η^f_{4j}
25	ϕ_{L3}	(1-[19]) (1-[31]-[37])	[19] (1-[22])
26	$\phi_{L3}-\phi_M$	(1-[19]) [37]	[19] [22]
27	$\phi_{L3}-\phi_M-\phi_M$	(1-[19]) [31]	–

where:

[19] = (L3:F)   [31] = (A:M+M|L3:A)

[22] = (F:M|L3:F)   [37] = (A:M+N|L3:A)

Table VI.5 Line Radiation from M-Shell Ionization, Fig. 7(a)

INDEX j	ENERGY	η^e_{5j}	η^f_{5j}
28	ϕ_M	1-[18]	[18]

where:

[18] = (M:F)

VII. INCOHERENT PHOTON SCATTERING AND COMPTON ELECTRON PRODUCTION

In both the CEPXS and ITS codes, the Klein-Nishina scattering cross section is used to represent the incoherent scattering of photons with atomic electrons. The Klein-Nishina cross section was derived for scattering with free or unbound electrons. The assumption that the photon collides with an unbound atomic electron is not valid for photons with energies on the order of the atomic binding energies [BIGGS1]. However, photoelectric absorption interactions dominate incoherent scattering at such energies. Both codes also ignore coherent scattering [BIGGS2]. The Klein-Nishina cross section is also in both codes to model the production of Compton electrons.

VII.1 THE KLEIN-NISHINA CROSS SECTION FOR PHOTON SCATTERING

The Klein-Nishina cross section for unpolarized, incoherent photon scattering is differential in the angle of the scattered photon relative to the incident photon's direction [MARM]. The microscopic form of this cross section for an interaction with an atomic electron is (in units of $cm^2 sr^{-1}$/electron):

$$\frac{d\xi^{KN}(T,\theta_\gamma)}{d\Omega_\gamma} = \frac{r_0^2}{2} \left(\frac{T'}{T}\right)^2 \left[\frac{T}{T'} + \frac{T'}{T} - \sin^2\theta_\gamma \right] \qquad (VII.1)$$

where:

T = The energy of the incident photon in reduced energy units.

T' = The energy of the scattered photon in reduced energy units. T' can vary from T (for $\mu_\gamma = 1$) to $T/(1+2T)$ (for $\mu_\gamma = -1$)

and,

$$\mu_\gamma = 1 + \frac{1}{T} - \frac{1}{T'} \qquad (VII.2)$$

Since the angle of scatter is kinematically determined by the energy at which the scattered photon emerges from the interaction, the Klein-Nishina cross section may also be expressed as a cross section that is differential in energy. In this case, the microscopic form of the Klein-Nishina cross section (in units of cm^2/electron per reduced photon energy) is:

$$\frac{d\xi^{KN}(T,T')}{dT'} = \frac{\pi r_0^2}{T^2} \left[\frac{T}{T'} + \frac{T'}{T} - 2\left(\frac{1}{T'} - \frac{1}{T} \right) + \left(\frac{1}{T'} - \frac{1}{T} \right)^2 \right] \qquad (VII.3)$$

Because energy and angle are kinematically related, the Klein-Nishina cross section for photon scattering that is differential in both energy and angle is given by:

$$\frac{d\xi^{KN}}{dT'd\Omega_\gamma} = \frac{d\xi^{KN}}{dT'} \frac{1}{2\pi} \delta\left(\mu - \mu_\gamma\right)$$

Hence, the expansion coefficients of the transfer matrices associated with photon incoherent scattering are:

FOR L = 0,1,...LMAX:

FOR f' = f, f+1, ... F : (VII.4)

$$\xi^{KN}_{f\to f',L} = \frac{1}{\Delta T_f} \int_{T_{f+1}}^{T_f} dT \int_{Max\left[T_{f'+1}, \frac{T}{(1+2T)}\right]}^{T_{f'}} dT' \; H(\Delta T') \; P_L(\mu_\gamma) \; \frac{d\xi^{KN}(T,T')}{dT'}$$

where the argument of the step function is:

$$\Delta T' = T_{f'} - Max\left[T_{f'+1}, \frac{T}{(1+2T)} \right]$$

and $\Delta T_f = T_f - T_{f+1}$.

The terms of the macroscopic transfer matrices for incoherent scattering are related to the terms of the microscopic transfer matrices by:

$$\sigma^{KN}_{f\to f',L} = \left(\frac{Z}{A}\right)_{eff} N_A \; \xi^{KN}_{f\to f',L} \qquad (VII.5)$$

As has been pointed out by Renken, et. al. [DTF], numerical integration of the Klein-Nishina cross sections is susceptible to inaccuracies due to the numerical cancellation. These problems can occur if the Legendre order is large (L>3), if the photon energy small ($E_f < 10$ keV), or if the photon group width is small.

Most of these difficulties can be avoided if the terms of the transfer matrices are not calculated to the maximum Legendre order, LMAX. For instance, the Klein-Nishina cross section becomes significantly

anisotropic only at higher energies (> 100 kev) [RENKEN]. Hence, for photons in the lower energy groups, only a few of the Legendre moments need to be calculated.

The Legendre moments of the Klein-Nishina cross sections are:

$$\sigma_{f,L}^{KN} = \sum_{f'} \sigma_{f \to f',L}^{KN} \qquad (VII.6)$$

In CEPXS, we perform the following test on these Legendre moments in order to avoid potential numerical difficulties in calculating the terms of the incoherent transfer matrices. If the ratio:

$$\sigma_{f,L}^{KN} \Big/ \sigma_{f,0}^{KN} \qquad (VII.7)$$

is less than .01, the higher-order expansion coefficients that represent photon-to-photon incoherent scattering are set to zero:

$$\sigma_{f \to f',L+1}^{KN} = 0$$

$$\sigma_{f \to f',L+2}^{KN} = 0 \qquad (VII.8)$$

$$\circ$$
$$\circ$$
$$\circ$$

$$\sigma_{f \to f',LMAX}^{KN} = 0$$

The total cross sections for incoherent scattering are:

FOR L = 0,1,...LMAX:
FOR f' = f, f+1, ... F:

$$\sigma_{t,f}^{KN} = \frac{1}{\Delta T_f} \int_{T_{f+1}}^{T_f} dT \int_{\frac{T}{1+2T}}^{T} dT' \; \frac{d\sigma^{KN}(T,T')}{dT'} \qquad (VII.9)$$

The effective absorption cross sections due to incoherent scattering are:

$$\sigma_{a,f}^{KN} = \sigma_{t,f}^{KN} - \sum_{f'} \sigma_{f \to f',0}^{KN} \qquad \text{(VII.10)}$$

The effective energy deposition cross sections due to incoherent photon scattering are:

$$\sigma_{E,f}^{KN} = \sigma_{t,f}^{KN} E_f^m - \sum_{f'} \sigma_{f \to f',0}^{KN} E_{f'}^m \qquad \text{(VII.11)}$$

VII.2 COMPTON ELECTRON PRODUCTION

The Klein-Nishina cross section for electron production can be written as differential in the angle of emission of the Compton electron relative to the incident photon's direction. The microscopic form of this cross section [MARM] for an interaction with an __atomic electron__ is (in units of $cm^2 sr^{-1}$/electron):

$$\frac{d\xi^{CO}(T,\theta_e)}{d\Omega_e} = \frac{(1+T)^2 (1-\mu_\gamma)^2}{\mu_e^3} \frac{r_0^2}{2} \left(\frac{T'}{T}\right)^2 \left(\frac{T}{T'} + \frac{T'}{T} - \sin^2\theta_\gamma\right) \qquad \text{(VII.12)}$$

where:

$$\mu_e = \frac{1+T}{T} \frac{1}{(2/\epsilon + 1)^{1/2}}$$

and ϵ is the kinetic energy of the Compton electron in reduced energy units. The energy of a Compton electron ranges from zero (at $\mu_\gamma = 1$) to

$$\frac{2T^2}{1+2T}$$

(at $\mu_\gamma = -1$). The Compton electron production cross section can also be cast into a form that is differential in the kinetic energy of the electron. In this case, the microscopic form of the Klein-Nishina cross section (in units of cm^2/electron per reduced electron energy) is:

$$\frac{d\xi^{CO}(T,\epsilon)}{d\epsilon} = \left|\frac{d\Omega_e}{d\epsilon}\right| \frac{d\xi^{CO}(T,\theta_e)}{d\Omega_e}$$

$$\text{(VII.13)}$$

$$= \frac{\pi r_0^2}{\epsilon^2} \left(1 - \frac{T'}{T}\right)^2 \left[\frac{T}{T'} + \frac{T'}{T} - 2\left(\frac{1}{T'} - \frac{1}{T}\right) + \left(\frac{1}{T'} - \frac{1}{T}\right)^2\right]$$

Because energy and angle are kinematically related, the Klein-Nishina cross section for electron production that is differential in both energy and angle is given by:

$$\frac{d\xi^{CO}}{d\epsilon d\Omega_e} = \frac{d\xi^{CO}}{d\epsilon} \frac{1}{2\pi} \delta\left(\mu - \mu_e\right)$$

For Compton electron production per collision with an <u>atomic electron</u>, the expansion coefficients of the transfer matrices are:

FOR L = 0,1,...LMAX: (VII.14)

FOR g = 1, 2, ... G :

$$\xi^{CO}_{f\to g,L} = \frac{1}{\Delta T_f} \int_{T_{f+1}}^{T_f} dT \int_{\epsilon_{g+1}}^{Min\left[\epsilon_g, \frac{2T^2}{1+2T}\right]} d\epsilon\ H(\Delta\epsilon)\ P_L(\mu_e)\ \frac{d\xi^{CO}(T,\epsilon)}{dT'}$$

where the argument of the step function is:

$$\Delta\epsilon = Min\left[\epsilon_g, \frac{2T^2}{1+2T}\right] - \epsilon_{g+1}$$

The terms of the macroscopic transfer matrices for Compton electron production are related to the terms of the microscopic transfer matrices by:

$$\sigma^{CO}_{f\to g',L} = \left(\frac{Z}{A}\right)_{eff} N_A\ \xi^{CO}_{f\to g',L}$$ (VII.15)

The cross section for Compton electron production becomes significantly anisotropic for photons of high energies [MARM]. Hence, only a few Legendre moments need to be calculated for the lower-energy photon groups.

The Legendre moments of the Compton production cross section are:

$$\sigma^{CO}_{f,L} = \sum_g \sigma^{CO}_{f\to g,L}$$ (VII.16)

In CEPXS, we perform the following test to avoid calculating the terms of the transfer matrices to excessive order. If the ratio:

$$\sigma_{f,L}^{CO} \Big/ \sigma_{f,0}^{CO} \qquad \text{(VII.17)}$$

is less than .01, the terms of the higher-order expansion coefficients that represent Compton production from group (f) are set to zero:

$$\sigma_{f \to g, L+1}^{KN} = 0$$

$$\sigma_{f \to g, L+2}^{KN} = 0 \qquad \text{(VII.18)}$$
$$\circ$$
$$\circ$$
$$\circ$$
$$\sigma_{f \to g, LMAX}^{KN} = 0$$

The effective energy deposition cross sections associated with Compton electron production are:

$$\sigma_{E,f}^{CO} = - \sum_{g} \sigma_{f \to g, 0}^{CO} \; E_g^m \qquad \text{(VII.19)}$$

The charge deposition cross sections for Compton production are:

$$\sigma_{C,f}^{CO} = - \sum_{g} \sigma_{f \to g, 0}^{CO} \qquad \text{(VII.20)}$$

and the secondary production cross sections for such interactions are:

$$\sigma_{S,f}^{CO} = \sum_{g} \sigma_{f \to g, 0}^{CO} \qquad \text{(VII.21)}$$

VIII. PHOTOELECTRIC ABSORPTION, PHOTOELECTRON PRODUCTION AND PHOTOELECTIC IONIZATION/RELAXATION PRODUCTION

Both CEPXS and ITS use the Biggs-Lighthill formulation [BIGGS3] for the photoelectric absorption cross section. The latest Biggs-Lighthill parameter set [BIGGS4] is not currently used in CEPXS.

VIII.1 <u>PHOTOELECTRIC ABSORPTION</u>

The photoelectric absorption cross section, in units of cm^2/g, can be expressed as a four-parameter fit [BIGGS3]:

$$\sigma^{PA}(E) = \sum_{k=1}^{4} C_k E^{-k} \tag{VIII.1}$$

where (E) is the energy of the photon in keV.

This cross section is defined as the probability per unit pathlength that photoionization occurs <u>in any shell</u>. The total cross sections associated with photoelectric absorption are:

$$\sigma^{PA}_{t,f} = \frac{\int_{E_{f+1}}^{E_f} dE \; \sigma^{PA}(E)}{\Delta E_f} \tag{VIII.2}$$

For photoelectric absorption, the absorption cross section is identical to the total cross section:

$$\sigma^{PA}_{a,f} = \sigma^{PA}_{t,f} \tag{VIII.3}$$

The effective energy deposition cross sections associated with photoelectric absorption are:

$$\sigma^{PA}_{E,f} = \sigma^{PA}_{a,f} E_f^m \tag{VIII.4}$$

VIII.2 <u>THE PRODUCTION OF PHOTOELECTRONS</u>

A photoelectric interaction produces an electron with kinetic energy equal to the energy of the photon less the binding energy of the shell that was ionized. The cross section for photoelectric production can be

separated into a cross section that is differential in the energy of the electron and a normalized angular distribution:

$$\frac{d\sigma^{PE}(E,\epsilon)}{d\epsilon d\Omega} = \sum_{i=1}^{6} \frac{dW^i(\theta,\epsilon)}{d\Omega} \frac{d\sigma^{PE,i}(E,\epsilon)}{d\epsilon} \qquad (VIII.5)$$

where:

    i = The shell index (i=1,2,3,4,5,6 : K,L1,L2,L3,"average" M, "effective" N),

    E = The energy of the photon,

    ϵ = The kinetic energy of the photoelectron = $E - \phi_i$,

    Ω = The angle at which the photoelectron is emitted relative to the direction of the photon,

    W^i = The differential angular distribution of photoelectrons produced by ionization of the i-th shell,

    ϕ_i ≡ The binding energy of the i-th shell in MeV.

The outer shells of an atom (N-shell and beyond) are considered to have zero binding energy in CEPXS. A photoelectric interaction with these shells produces electrons with the same energy as the photon. As far as CEPXS is concerned, the "effective" N-shell includes all the outer shells of an atom. Note also that an ionization cross section (Eq. V.2) is not calculated for these outer shells since a vacancy in one of these shells does not induce relaxation radiation in CEPXS.

The photoelectric production cross section is:

$$\frac{d\sigma^{PE,i}(E,\epsilon)}{d\epsilon} = \chi_i(E) \; \sigma^{PA}(E) \; \delta(\epsilon-E+\phi_i) \qquad (VIII.6)$$

where:

$\chi_i(E)$ = The probability that a photon of energy E ionizes the i-th shell.

The photoionization probability, χ_i, can be evaluated in terms of photoeffect efficiencies, f_i. These are defined using the values of the photoelectric cross section immediately above and below the shell

binding energy [SANDYL] in the following manner:

$$f_i = 1 - \frac{\sigma^{PA}(\phi_i - \delta)}{\sigma^{PA}(\phi_i + \delta)} \qquad \text{(VIII.7)}$$

where δ is an arbitrarily small energy increment. In CEPXS, δ is taken to be one keV for the numerical calculation of photoeffect efficiencies.

The photoeffect efficiency denotes the probability that photoionization will occur in the i-th shell provided that photoionization has not occured in any of the shells with larger binding energies than ϕ_i. With the NO-PCODE option, only the K-shell photoeffect efficiency, f_1, is employed. It is calculated using the Biggs-Lighthill photoelectric cross section. In the default version of CEPXS, the photoeffect efficiencies can be expressed in terms of relaxation quantity data obtained from ITS:

$$f_1 = 1 - [9] \quad ,$$

$$f_2 = 1 - [13] \quad ,$$

$$f_3 = 1 - [14] \quad , \qquad \text{(VIII.8)}$$

$$f_4 = 1 - [15] \quad ,$$

$$f_5 = 1 - [16] \quad ,$$

$$f_6 = 1.0$$

where the bracketed numerals are the indices of the relaxation quantities obtained from ITS [HALB].

The photoionization probability of the six shells can be expressed in terms of these photoeffect efficiencies as:

$$\chi_1(E) = f_1 \quad \text{if } E > \phi_1$$
$$= 0 \quad \text{if } \phi_1 > E$$

$$\chi_2(E) = (1-f_1)f_2 \quad \text{if } E > \phi_1$$
$$= f_2 \quad \text{if } \phi_1 > E > \phi_2$$
$$= 0 \quad \text{if } \phi_2 > E$$

$$\text{(VIII.9)}$$

$$\chi_3(E) = (1-f_1)(1-f_2)f_3 \quad \text{if } E > \phi_1$$
$$= (1-f_2)f_3 \qquad \text{if } \phi_1 > E > \phi_2$$
$$= f_3 \qquad \text{if } \phi_2 > E > \phi_3$$
$$= 0 \qquad \text{if } \phi_3 > E$$

$$\chi_4(E) = (1-f_1)(1-f_2)(1-f_3)f_4 \quad \text{if } E > \phi_1$$
$$= (1-f_2)(1-f_3)f_4 \qquad \text{if } \phi_1 > E > \phi_2$$
$$= (1-f_3)f_4 \qquad \text{if } \phi_2 > E > \phi_3$$
$$= f_4 \qquad \text{if } \phi_3 > E > \phi_4$$
$$= 0 \qquad \text{if } \phi_4 > E$$

$$\chi_5(E) = (1-f_1)(1-f_2)(1-f_3)(1-f_4)f_5 \quad \text{if } E > \phi_1$$
$$= (1-f_2)(1-f_3)(1-f_4)f_5 \qquad \text{if } \phi_1 > E > \phi_2$$
$$= (1-f_3)(1-f_4)f_5 \qquad \text{if } \phi_2 > E > \phi_3$$
$$= (1-f_4)f_5 \qquad \text{if } \phi_3 > E > \phi_4$$
$$= f_5 \qquad \text{if } \phi_4 > E > \phi_5$$
$$= 0 \qquad \text{if } \phi_5 > E$$

$$\chi_6(E) = (1-f_1)(1-f_2)(1-f_3)(1-f_4)(1-f_5)f_6 \quad \text{if } E > \phi_1$$
$$= (1-f_2)(1-f_3)(1-f_4)(1-f_5)f_6 \qquad \text{if } \phi_1 > E > \phi_2$$
$$= (1-f_3)(1-f_4)(1-f_5)f_6 \qquad \text{if } \phi_2 > E > \phi_3$$
$$= (1-f_4)(1-f_5)f_6 \qquad \text{if } \phi_3 > E > \phi_4$$
$$= (1-f_5)f_6 \qquad \text{if } \phi_4 > E > \phi_5$$
$$= f_6 \qquad \text{if } \phi_5 > E > \phi_6$$
$$= 0 \qquad \text{if } \phi > E_6$$

Note that:

$$\sum_{i=1}^{6} \chi_i(E) = 1.0$$

The cross section transfer matrix associated with photoelectron

production are:

FOR L = 0,1,...LMAX:

FOR f = 1,2,...F:

$$\sigma^{PE}_{f \to g,L} = \sum_{i=1}^{6} W^i_L(\epsilon^m_g) \; \frac{\displaystyle\int_{E_{f+1}}^{E_f} dE \int_{\epsilon_{g+1}}^{\epsilon_g} d\epsilon \; \frac{d\sigma^{PE,i}(E,\epsilon)}{d\epsilon}}{\Delta E_f} \qquad (VIII.10)$$

or:

$$\sigma^{PE}_{f \to g,L} = \sum_{i=1}^{6} W^i_L(\epsilon^m_g) \; \frac{\displaystyle\int_{Max\left[E_{f+1}, \; \epsilon_{g+1} + \phi_i\right]}^{Min\left[E_f , \; \epsilon_g + \phi_i\right]} H(\Delta E) \; \chi_i(E) \; \sigma^{PA}(E) \; dE}{\Delta E_f}$$

$$(VIII.11)$$

where the argument of the step function is:

$$\Delta E = Min \left[E_f , \; \epsilon_g + \phi_i\right] - Max\left[E_{f+1}, \; \epsilon_{g+1} + \phi_i\right]$$

Two different normalized angular distributions for the photoelectrons are used in CEPXS. For low-energy photoelectrons, the Fischer distribution [DAVISS] is used:

$$\frac{dW^i(\theta,\epsilon)}{d\Omega} = \frac{1}{2\pi} \frac{dW^i(\theta,\epsilon)}{d\theta} = \frac{3\left[1-b^2\right]^2 \sin^3\theta}{8\pi \; (1-b \; \cos\theta)^4} \qquad (VIII.12)$$

where:

$$b = \frac{\beta}{1 + \dfrac{\epsilon + \phi_i}{1.022}}$$

and all energies are expressed in terms of MeV, and ϕ_i is the binding energy of the shell that was ionized by photoelectric absorption.

For high-energy photoelectrons, the Sauter distribution [DAVISS] is used:

$$\frac{dW(\theta,\epsilon)}{d\Omega} = \frac{1}{2\pi} \frac{dW(\theta,\epsilon)}{d\theta} = \frac{A}{2\pi}\left[\frac{\beta^2(1-\beta^2)^{1/2}\sin^3\theta}{(1-\beta\cos\theta)^4} + \frac{\left(1+ (1-\beta^2)^{1/2}\right)^2\beta^2\sin^3\theta}{2\ (1-\beta^2)\ (1-\beta\cos\theta)^3} \right]$$

(VIII.13)

where:

$$A = \left[\frac{4\beta^2(1-\beta^2)^{1/2}}{3\ (1-\beta^2)^2} + \frac{\left(1+ (1-\beta^2)^{1/2}\right)^2\beta^2}{2\ (1-\beta^2)}\left\{ \frac{2}{\beta^2(1-\beta^2)} - \frac{1}{\beta^2}\ \text{Log}\ \left(\frac{1+\beta}{1-\beta} \right) \right\} \right]^{-1}$$

Note that the Sauter distribution depends only on the energy of the photoelectron and not on the binding energy of the shell that was ionized. Hence, the shell index superscript on the angular distribution in Eq. VIII.13 is suppressed.

In CEPXS, we follow the recommendation of MacCallum [MAC] that the choice between the Fischer and Sauter angular distributions be made in the following way:

$$\text{Fischer}\quad \text{IF}\ \epsilon \leq .0025\ Z - .5 * \phi_1$$

$$\text{Sauter}\quad \text{IF}\ \epsilon > .0025\ Z - .5 * \phi_1$$

(VIII.14)

where ϕ_1 is the binding energy of the K-shell and all energies are in MeV.

The Legendre moments of the photoelectron angular distribution:

$$W_L^i(\epsilon) = 2\pi \int_0^\pi d\theta\ P_L(\cos\theta)\ \frac{dW^i(\epsilon,\theta)}{d\theta}$$

(VIII.15)

are calculated by quadrature in CEPXS. The calculation of the multigroup-Legendre transfer matrix for photoelectron production (Eq. VIII.10) is simplified by evaluating the Legendre moments of the photoelectron angular distribution at the midpoint energy of the electron group.

The effective energy deposition cross sections associated with the production of photoelectrons are:

$$\sigma^{PE}_{E,f} = - \sum_g \sigma^{PE}_{f \to g,0} \; \epsilon^m_g \qquad \text{(VIII.16)}$$

The charge deposition cross sections associated with photoelectric production are:

$$\sigma^{PE}_{C,f} = - \sum_g \sigma^{PE}_{f \to g,0} \qquad \text{(VIII.17)}$$

and the secondary production cross sections for these interaction are:

$$\sigma^{PE}_{S,f} = \sum_g \sigma^{PE}_{f \to g,0} \qquad \text{(VIII.18)}$$

VIII.3 RELAXATION PRODUCTION

The same relaxation radiation cascade is produced whether ionization occurs by electron impact or the photoelectric effect. The multigroup photoionization cross section of the i-th shell is given by:

$$\sigma^{PI,i}_f = \frac{\int_{E_{f+1}}^{E_f} dE \; \chi_i(E) \; \sigma^{PA}(E)}{\Delta E_f} \qquad \text{(VIII.19)}$$

The expansion coefficients of the transfer matrix associated with electron relaxation radiation production resulting from photoionization are:

FOR f = 1,2,...F:

$$\sigma^{PIE}_{f \to g,0} = \sum_{i=1}^{5} \sum_{j=1}^{28} \eta^e_{ij} \; \delta_{gg_j} \; \sigma^{PI,i}_f \qquad \text{(VIII.20)}$$

where: i = The shell index,

j = The index associated with line radiation,

η^e_{ij} = The relaxation efficiency that the electrons of line index j will be produced following ionization of the ith shell,

g_j = The electron group that contains the energy of the jth Auger electron

The expansion coefficients of transfer matrix associated with fluorescence production resulting from impact ionization are:

FOR $f = 1,2,\ldots F$:

$$\sigma^{PIF}_{f \rightarrow f',0} = \sum_{i=1}^{5} \sum_{j=1}^{28} \eta^{f}_{ij} \; \delta_{f'f_j} \; \sigma^{PI,i}_{f} \qquad (VIII.21)$$

where:

η^{f}_{ij} = The relaxation efficiency that a fluorescence photon of line index j will be produced following ionization of the ith shell,

f_j = The photon group that contains the energy of the jth fluorescence photon.

The energy deposition cross sections associated with the production of relaxation radiation by photoionization are:

$$\sigma^{PI}_{E,f} = - \sum_{g} \sigma^{PIE}_{f \rightarrow g,0} \; E^{m}_{g} \; - \sum_{f'} \sigma^{PIF}_{f \rightarrow f',0} \; E^{m}_{f'} \qquad (VIII.22)$$

The charge deposition cross sections associated with the production of relaxation radiation by photoionization are:

$$\sigma^{PI}_{C,f} = - \sum_{g} \sigma^{PIE}_{f \rightarrow g,0} \qquad (VIII.23)$$

The secondary production cross section associated with the production of relaxation radiation following photoionization is:

$$\sigma^{PI}_{S,f} = \sum_{g} \sigma^{PIE}_{f \rightarrow g,0} \; + \sum_{f'} \sigma^{PIF}_{f \rightarrow f',0} \qquad (VIII.24)$$

IX. PAIR ABSORPTION AND SECONDARY PRODUCTION

Both CEPXS and ITS use the Biggs-Lighthill formulation for the pair absorption cross section.

IX.1 PAIR ABSORPTION

The pair absorption cross section, in units of cm^2/g-photon, can be expressed as a parameter fit [BIGGS5] in the following fashion:

$$\sigma^{PAA}(E) = 0.0 \qquad\qquad \text{IF } E < 1022 \text{ keV ,}$$

$$\sigma^{PAA}(E) = C \left[E - 1022\right] \qquad \text{IF } 1022 \text{ keV} < E < 1500 \text{ keV ,} \tag{IX.1}$$

$$\sigma^{PAA}(E) = \sum_{k=1}^{7} \frac{A_k \left[E - 1022\right]^k}{1.0 + 1.7(10^{-13}) \left[E - 1022\right]^3} \qquad \text{OTHERWISE,}$$

where E is the energy of the photon in keV. The Biggs-Lighthill cross section for pair absorption is valid up to 100 MeV.

The total cross sections associated with absorption from pair interactions are:

$$\sigma^{PAA}_{t,f} = \frac{\displaystyle\int_{E_{f+1}}^{E_f} dE \; \sigma^{PAA}(E)}{\Delta E_f} \tag{IX.2}$$

For absorptive interactions such as the pair interaction, the absorption cross section is identical to the total cross section:

$$\sigma^{PAA}_{a,f} = \sigma^{PAA}_{t,f} \tag{IX.3}$$

The effective energy deposition cross sections for pair interaction absorption are:

$$\sigma^{PAA}_{E,f} = \sigma^{PAA}_{a,f} E_f^m \tag{IX.4}$$

IX.2 THE PRODUCTION OF PAIR SECONDARIES

A pair interaction results in the production of a positron and an electron. The energies of the pair secondaries (in keV) are correlated in the following fashion:

$$\epsilon^- + \epsilon^+ = h\nu - 1022 \qquad \text{(IX.5)}$$

where ϵ^- is the energy of the pair electron, ϵ^+ is the energy of the pair positron, and $h\nu$ is the energy of the photon. The expression on the right side of Eq. IX.5 is the energy that is available for distribution to the pair secondaries. Both the positron and the electron can have kinetic energy that varies from zero to this maximum available energy.

The cross section for the production of a pair positron can be separated into three components: the total pair absorption cross section, a normalized distribution that is differential in the energy of the positron, and a normalized distribution that is differential in the angle of emission of the positron relative to the direction of the incident photon:

$$\frac{d\sigma^{P+}(E,\epsilon^+)}{d\epsilon^+ d\Omega} = \sigma^{PAA}(E) \frac{dW(\mu,\epsilon^+)}{d\Omega} \frac{df^{P+}(E,\epsilon^+)}{d\epsilon^+} \qquad \text{(IX.6)}$$

The cross section for the production of a pair electron is similar:

$$\frac{d\sigma^{P-}(E,\epsilon^-)}{d\epsilon^- d\Omega} = \sigma^{PAA}(E) \frac{dW(\mu,\epsilon^-)}{d\Omega} \frac{df^{P-}(E,\epsilon^-)}{d\epsilon^-} \qquad \text{(IX.7)}$$

The same angular distributions are used for both the electron and the positron. Since pair production occurs in the vicinity of a nucleus which acquires some of the momentum of the incident photon, the angles at which the pair secondaries are emitted are not correlated.

Since bremsstrahlung and pair production are inverse processes, the same angular distribution can be used for pair secondaries as was used for bremsstrahlung photons (cf. Eq. III.14):

$$\frac{dW(\mu,\epsilon)}{d\Omega} = \frac{1}{2\pi} \frac{dW(\mu,\epsilon)}{d\mu} = \frac{1 - \beta^2}{4\pi (1-\beta\mu)^2} \qquad \text{(IX.7)}$$

Just as the bremsstrahlung angular distribution becomes more forward peaked as the incident electron's energy increases, the angular

distribution of pair secondaries becomes increasingly forward peaked as
the incident photon's energy increases. The recursion relation for the
Legendre moments of the bremsstrahlung distributions (Chapter III) are
used to evaluate the Legendre moments of this distribution.

Both pair secondaries have the same distribution in energy:

$$\frac{df^{P-}(E,\epsilon^-)}{d\epsilon^-} = \frac{df^{P+}(E,\epsilon^+)}{d\epsilon^+} \qquad (IX.8)$$

The energy distribution of the pair secondaries is given by Bethe-
Heitler theory [BETHE]. In CEPXS, tabulated values for this
distribution at selected photon energies were obtained from a text
[MARM]. The energy distribution of the pair secondaries are tabulated
up to a photon energy of 100 MeV on one of the cross section data tapes
accessed by CEPXS.

In Fig. 8, the energy distribution of the pair secondaries is shown for
five different photon energies. The distribution is plotted as a
function of the fraction:

$$x = \frac{\epsilon}{h\nu - 2m_e c^2}$$

of the available energy possessed by the pair secondary. Since either
the electron or the positron can emerge with all of the available
energy, this fraction can vary from zero to unity.

Only half of the energy distribution function is shown in Fig. 8. The
rest of the distribution is symmetric about $x = 0.5$. This symmetry
reflects the correlation in energy of the positron and the electron
described in Eq. IX.5. Not shown in the Figure 5 are curves for this
distribution at two other photon energies that are tabulated in CEPXS:
at $h\nu = 1.53$ MeV, the distribution is the same as that at $h\nu = 5.11$ MeV
and at $h\nu = 1.02$ MeV, the distribution function is unity for all x. For
a particular photon energy and a particular secondary particle energy,
the value of the distribution function is obtained in CEPXS by a two-
dimensional interpolation of this seven curve set.

The expansion coefficients of transfer matrices for pair electron
production are:

FOR L = 0,1,...LMAX:
FOR f = 1,2,..F:

$$\sigma_{f \to g,L}^{P-} = \frac{1}{\Delta E_f} \int_{E_{f+1}}^{E_f} dE \int_{\epsilon_{g+1}}^{\epsilon_g} d\epsilon \ \sigma^{PPA}(E) \ W_L(E_g^m) \ \frac{df^{P-}(E,\epsilon)}{d\epsilon} \qquad \text{(IX.9)}$$

Note that the angular distribution of the pair electrons is evaluated in at the midpoint energy of the electron group.

The transfer matrices for positron pair production are the same as those for electron pair production:

$$\sigma_{f \to h,L}^{P+} = \sigma_{f \to g,L}^{P-} \qquad \text{(IX.10)}$$

The effective energy deposition cross sections associated with the pair production of electrons and positrons are:

$$\sigma_{E,f}^{P-} = -\sum_g \sigma_{f \to g,0}^{P-} E_g^m$$

$$\text{(IX.11)}$$

$$\sigma_{E,f}^{P+} = -\sum_h \sigma_{f \to h,0}^{P+} E_h^m$$

The secondary production cross sections associated with the pair production of electrons and positrons are:

$$\sigma_{S,f}^{P-} = \sum_g \sigma_{f \to g,0}^{P-}$$

$$\text{(IX.12)}$$

$$\sigma_{S,f}^{P+} = \sum_h \sigma_{f \to h,0}^{P+}$$

X. POSITRON INTERACTIONS

The same elastic scattering, inelastic scattering, and impact ionization cross sections are used for both electrons and positrons in CEPXS. Positron specific cross sections (e.g the inelastic Bhabba scattering cross section [BHABBA]) are not implemented in CEPXS.

Unlike electrons, positrons can undergo annihilation reactions. Both ITS and CEPXS allow annihilation to occur only when the positron is "absorbed". That is, annihilation occurs when the energy of the positron becomes less than the cutoff energy, E_{G+1}. In the annihilation process, two photons, each possessing the energy equivalent to the rest mass of an electron, are produced. These annihilation quanta are emitted isotropically. The transfer matrix associated with the production of annihilation radiation consists of the following terms:

$$\sigma^{ANN}_{h \to f, 0} = 2.0 \; \Sigma^P_{a,h} \; \delta_{ff'} \qquad (X.1)$$

where f' is the photon energy group into which the annihilation quanta are produces.

The secondary and energy deposition cross sections associated with the production of annihilation radiation are:

$$\sigma^{ANN}_{S,h} = 2.0 \; \sigma^P_{a,h}$$

$$\sigma^{ANN}_{E,h} = -2.0 \; E^m_{f'} \; \sigma^P_{a,h} \qquad (X.2)$$

XI. COMPARISON TO ITS

The models used in CEPXS and ITS (Version 2.1) for electron interactions are compared in Table XI.1.

Table XI.1 Electron interactions in CEPXS and ITS

INTERACTION	CEPXS	ITS
Inelastic Collisional Scattering	Moller cross section for catastrophic collisional energy losses and restricted CSD for soft energy losses	Condensed history for all collisional energy losses
Energy-loss Straggling	Implicit for catastrophic collisions and none for soft collisions	Explicit in condensed-history for all collisions
Deflection of primaries	Truncated Legendre expansion	Included in elastic scattering cross section
Knock-on Production	Moller cross section	Moller cross section
Knock-on Correlation with Primaries	Correlation with primaries from catastrophic collisions	No correlation between knock-ons and primaries
Collisional Stopping Power	Bethe stopping power with the Sternheimer density effect correction and extrapolation of the stopping power below 10 keV	Bethe stopping power with the Sternheimer density effect correction
Radiative Emission	Simple bremsstrahlung cross section	Complex bremsstrahlung cross section by default
Inelastic Radiative	Bremsstrahlung cross section for catastrophic radiative	Bremsstrahlung cross section for all

Scatter	energy losses and restricted CSD for soft radiative energy losses	radiative energy losses
Energy-loss Straggling	Implicit for catastrophic radiative events and none for soft radiative events	Implicit for all radiative events
Deflection of electron by radiative emission	None	None
Bremsstrahlung Correlation	Scattered electrons correlated with bremsstrahlung for catastrophic events but not for soft radiative events	Correlation between all radiatively scattered electrons and bremsstrahlung
Elastic Scattering	Mott cross section with Moliere screening for E > 256 keV and Riley cross sections used for E < 256 keV	Mott cross section with Moliere screening for for E > 256 keV and Riley cross sections for E < 256 keV
	Single-event cross sections with the extended transport correction	Goudsmit-Saunderson condensed-history distribution
Impact Ionization/ Relaxation	Kolbenstvedt cross section for NO-PCODE option. Gryzinski cross section by default	Kolbenstvedt cross section by default. Gryzinski cross section for PCODE option
Correlation with knock-on production	None	None
Relaxation	Only from K-shell with NO-PCODE option	Only from K-shell by default
	From K,L1,L2,L3, average M shells by default	From K,L1,L2,L3, average M, and average N shells for PCODE option

The models used in CEPXS and ITS for photon interactions are compared in Table XI.2.

Table XI.2 Photon Interactions in CEPXS and ITS

INTERACTION	CEPXS	ITS
Incoherent Scattering	Klein-Nishina	Klein-Nishina
Coherent Scattering	None	None
Compton electron production	Klein-Nishina	Klein-Nishina
Photoelectric Absorption	Biggs-Lighthill	Biggs-Lighthill
Photoelectric Production	Photoeffect efficiencies from data tape Fischer and Sauter angular distributions	Photoeffect efficiencies from data tape Fischer and Sauter angular distributions
Pair Absorption	Biggs-Lighthill	Biggs-Lighthill
Pair Production	Sommerfield angular distribution Bethe-Heitler theory for energy distribution	Sommerfield angular distribution Bethe-Heitler theory for energy distribution

XII. GLOSSARY

Some of the terms used frequently in this report are given below along with the units in which they appear in CEPXS.

A_i $\equiv$ Gram-atomic weight of the ith element in a compound

β $\equiv v/c = [T(T+2)]^{1/2}/(T+1)$

ϵ $\equiv$ Photon energy in reduced energy units
    (i.e. in units of an electron rest mass)

ζ $\equiv$ Microscopic cross section (cm^2)

f $\equiv$ Group index for photons

g $\equiv$ Group index for electrons

h $\equiv$ Group index for positrons

$H(x)$ $= \begin{cases} 0 \text{ if } x \leq 0 \\ 1 \text{ if } x > 0 \end{cases}$

LMAX $\equiv$ Maximum Legendre order of cross sections

m_e $\equiv$ Rest mass of electron in g

$m_e c^2$ $\equiv$ Rest mass of electron in MeV

N_A $\equiv$ Avogardo's number $= 6.023 \times 10^{23}$

r_o $\equiv$ Classical electron radius $= 2.82e-13$ cm

ρ $\equiv$ Material density (g/cm^3)

σ $\equiv$ Macroscopic cross section (cm^2/g)

Σ $\equiv$ Aggregate macroscopic cross section (cm^2/g) for many
    interactions.

T $\equiv$ The kinetic energy of an electron in reduced energy units

w_i $\equiv$ Weight percent of the ith element in a compound

$Z_i \equiv$ Atomic number of the ith element in a compound

$$\left(\frac{Z}{A}\right)_{eff} \equiv \sum_i \frac{w_i Z_i}{A_i}$$

XIII. REFERENCES

[ASH]   J. C. Ashley and V. E. Anderson, IEEE Trans. Nucl. Sci., 28, 4132 (1981).

[BART] D. E. Bartine, R. G. Alsmiller, Jr., F. R. Mynatt, W. W. Engle, Jr., and J. Bariah, Nucl. Sci. and Eng., 48, 159 (1972).

[BELL] G. I. Bell and S. Glasstone, Nuclear Reactor Theory, (1970).

[BERG1] M. J. Berger and S. M. Seltzer, Phys. Rev. 2, 621 (1970).

[BERG2] M. J. Berger, "Monte Carlo Calculations of the Penetration and Diffusion of Fast Charged Particles," Methods of Computational Physics, 1, 135 (1963).

[BETHE] H. A. Bethe and J. Ashkin, Experimental Nuclear Physics, Vol. I, E. Segre, Ed., (1953).

[BHABBA] H. J. Bhabba, Proc. Roy. Soc. (London), A154, 195 (1936).

[BIGGS1] F. Biggs and R. Lighthill, "Analytical Approximations for Photon-Atom Differential Scattering Cross Sections Including Electron Binding Effects," SC-RR-72 0659 (1972).

[BIGGS2] F. Biggs and R. Lighthill, "Analytical Approximations for Total and Energy Absorption Cross Sections for Photon-Atom Scattering," SC-RR-72 0685 (1972).

[BIGGS3] F. Biggs and R. Lighthill, "Analytical Approximations for X-ray Cross Sections II," SC-RR-71 0507, Sandia National Laboratories (1971).

[BIGGS4] F. Biggs and R. Lighthill, "Analytical Approximations for X-ray Cross Sections III," SAND87 - 0070, Sandia National Laboratories (1988).

[BIGGS5] F. Biggs and R. Lighthill, "Analytical Approximations for Total Pair-Production Cross Sections," SC-RR-68-619, Sandia National Laboratories (1968).

[BURHOP] E. H. S. Burhop, J. Phys. Radium, 16, 625 (1955).

[DAVISS] C. M. Davisson and R. D. Evans, Rev. of Modern Phys., 24, 79 (1952).

[DEVA] J. J. Devaney, "Electron Stopping Powers of Some Elements and Compounds from 0 to 10,000 ev; A Compilation,," Los Alamos National Laboratory, LA-11625-MS (1989).

[DTF]   J. H. Renken, K. G. Adams, "An Improved Capability for Solution of Photon Transport Problems by the Method of Discrete Ordinates," SC-RR-69-739, (1969).

[ETRAN] M. J. Berger and S. M. Seltzer, "ETRAN Monte Carlo Code System for Electron and Photon Transport Through Extended Media," CCC-107, Oak Ridge National Laboratory (1968).

[GRYZ] Gryzinski, Phys. Rev., 138, A322 (1964).

[HAGE] H. Hagedoorn and A. H. Wapstra, Nuclear Physics,

[HALB] J. A. Halbleib and J. E. Morel, "Improved Atomic Shell Excitation and Relaxation in the TIGER Series of Codes," SAND78-0580, Sandia National Laboratories (1978).

[ICRU] Stopping Powers for Electrons and Positrons, ICRU Report 37 (1984).

[ITS] J. A. Halbleib and T. A. Mehlhorn, Nucl. Sci. and Eng., 92, (1986).

[KOCH] H. W. Koch and J. W. Motz, Rev. of Mod. Phys., 31, 920 (1959).

[KOLBEN] H. Kolbenstvedt, J. Appl. Phys., 38, 4785 (1967).

[LAZO] M. S. Lazo and J. E. Morel, Nucl. Sci. and Eng., 92, 98 (1986).

[MAC] C. J. MacCallum and T. A. Dellin, J. Appl. Phys., (1973).

[MARM] P. Marmier and E. Sheldon, PHYSICS OF NUCLEI AND PARTICLES, (1969).

[MOR1] J. E. Morel, Nucl. Sci. Eng., 71, 64 (1980).

[MOR2] J. E. Morel, Nucl. Sci. Eng., 79, 340 (1981).

[MOR3] J. E. Morel, Nucl. Sci. Eng., 91, 324 (1985).

[MOR4] J. E. Morel and L. J. Lorence, Trans. Am. Nucl. Soc., 52, 384 (1986).

[MOR5] J. E. Morel, Nucl. Sci. and Eng., 101, 72 (1989).

[MOR6] J. E. Morel and G. R. Montry, Transport Theory and Statistical Physics, 13, 615 (1984).

[ONET] T. R. Hill, "ONETRAN: A Discrete Ordinates Finite Element Code for the Solution of the One-Dimensional Multigroup Transport Equation," LA-5990-MS, Los Alamos National Laboratory (1975).

[ONED] ONEDANT: A One-Dimensional, Multigroup, Diffusion-Accelerated, Neutral Particle Transport Code, CCC-428, Oak Ridge National Laboratory Code Distribution Center, Oak Ridge TN.

[RAO] T. S. Rao-Sahib and D. B. Wittry, J. Appl. Phys., 45, 5060 (1974).

[RENKEN] J. Appl. Physics, $\underline{38}$, 4925 (1967).

[RILEY] M. E. Riley, C. J. MacCallum, and F. Biggs, Atomic Data and Nuclear Data Tables, $\underline{15}$, 443 (1975).

[SANDYL] $\underline{SANDYL}$, Sandia National Laboratories, SLL-74-0012 (1974).

[SHIM] R. Schimizu and S. Ichimura, Surface Science, $\underline{133}$, 250 (1982).

[SPENCE] L. V. Spencer, Phys. Rev., $\underline{98}$, 1507 (1955).

[STERN] R. M. Sternheimer, Phys. Rev. $\underline{103}$, 511 (1956).

[ZERBY] C. D. Zerby and F. L. Keller, Nucl. Sci. and Eng., $\underline{27}$, 190 (1967).

COLLISIONAL STOPPING POWER IN Au
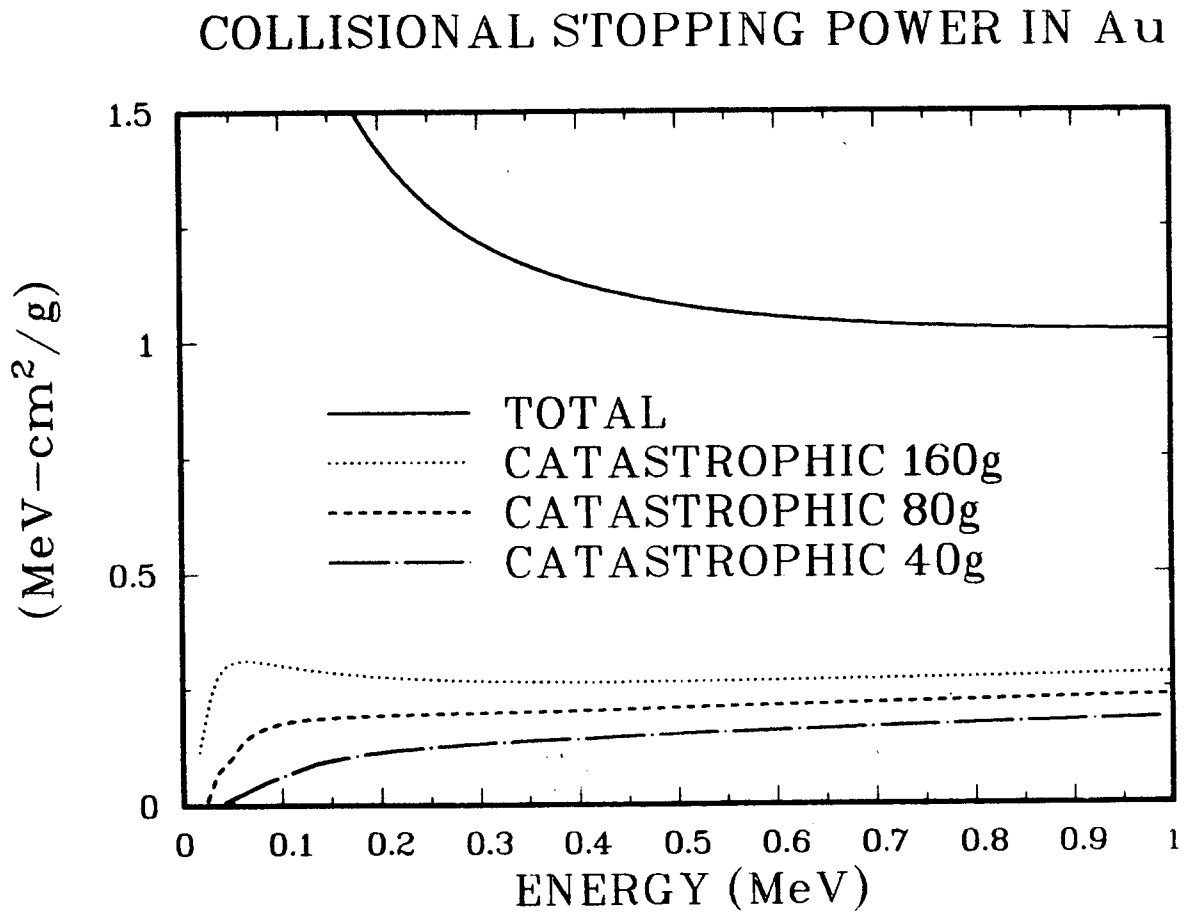
Fig. 1. The total collisional stopping power and the restricted collisional stopping power vs. energy in gold.
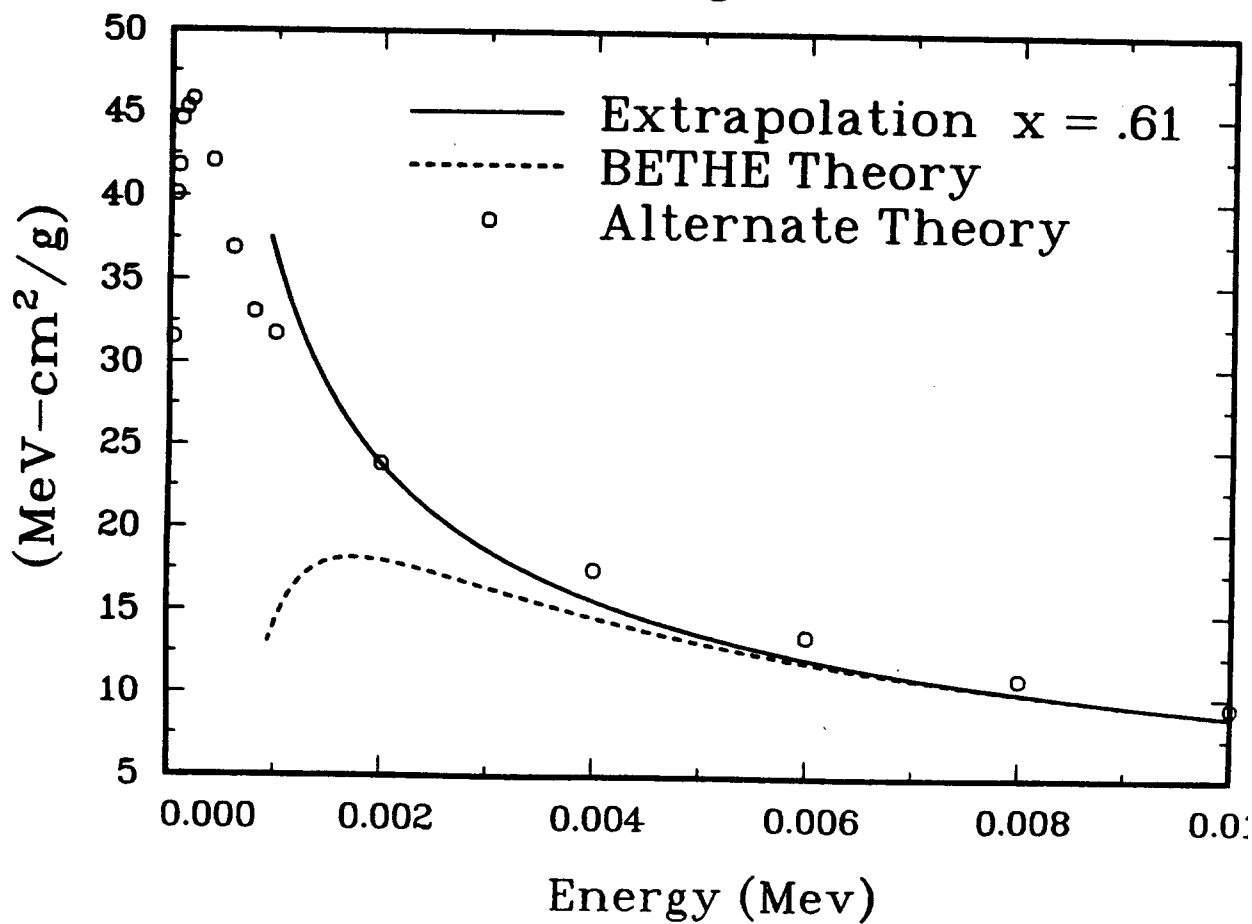
Fig. 2. The total collisional stopping power in tungsten below 10 keV according to Bethe theory, refined predictions, and the parabolic extrapolation used in CEPXS.

Total Collisional Stopping Power
Silicon
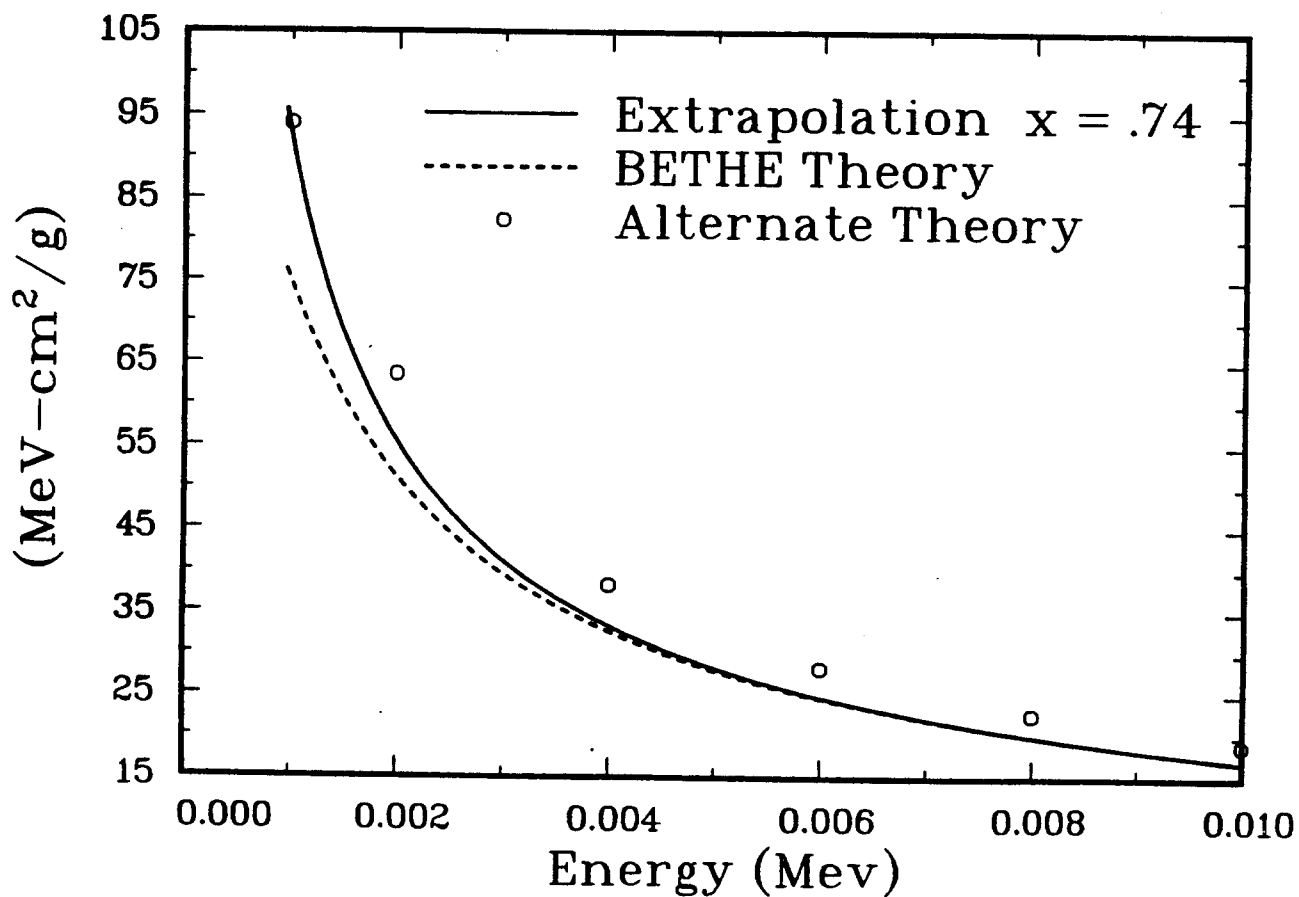
Fig. 3. The total collisional stopping power in silicon below 10 keV
according to Bethe theory, refined predictions, and the
parabolic extrapolation used in CEPXS.

STOPPING POWER EXTRAPOLATION
BELOW 10 keV
$$S \sim E^{-X}$$
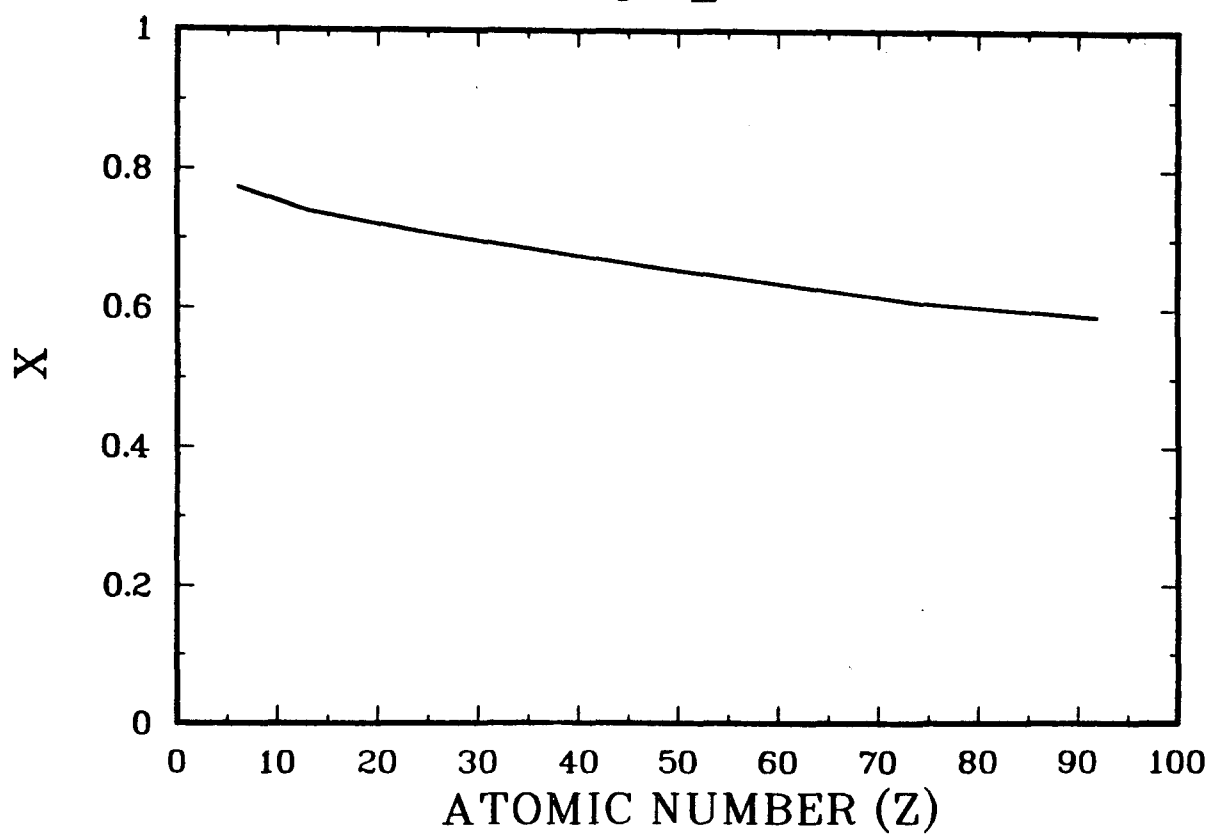
Fig. 4. The extrapolation parameter used in CEPXS below 10 keV as a function of atomic number.

Fig. 5. The total collisional stopping power in water vs. energy, with and without the density effect correction.

RADIATIVE STOPPING POWER IN Au
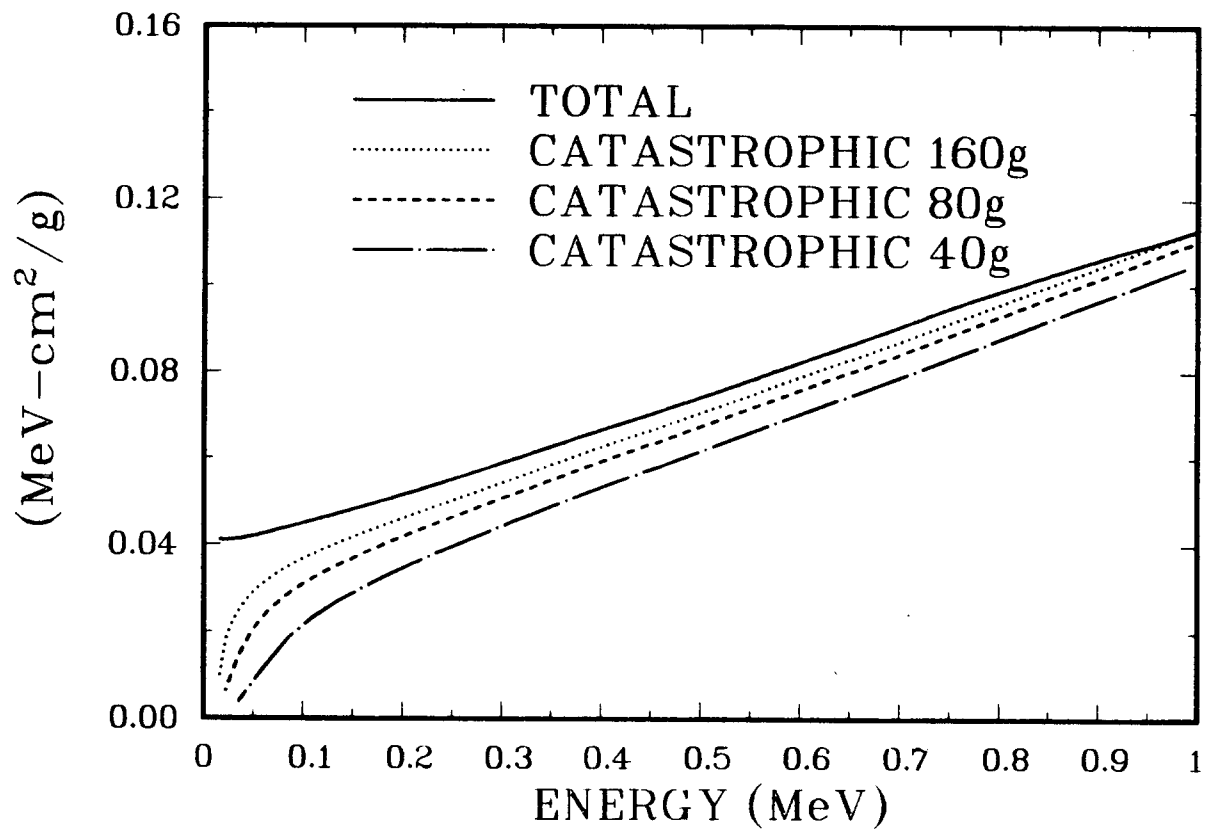
Fig. 6. The total radiative stopping power and the restricted radiative stopping power calculated with various numbers of groups, vs. energy in gold.
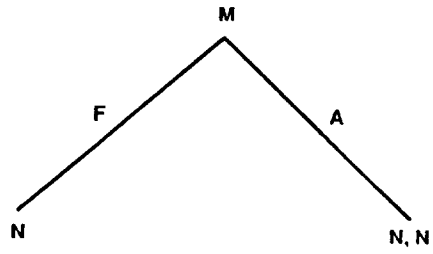
Fig. 7A. Relaxation cascade from the average M shell.
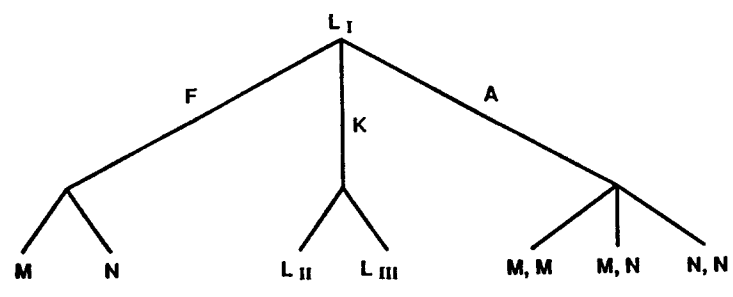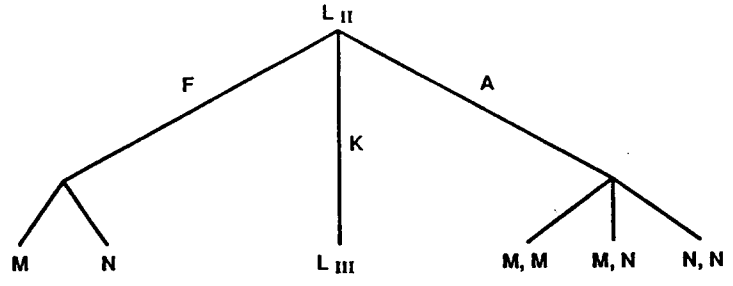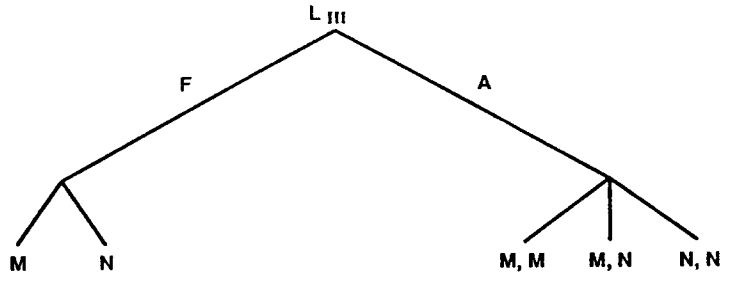
Fig. 7B. Partial relaxation cascades from the L1, L2, L3 shells.
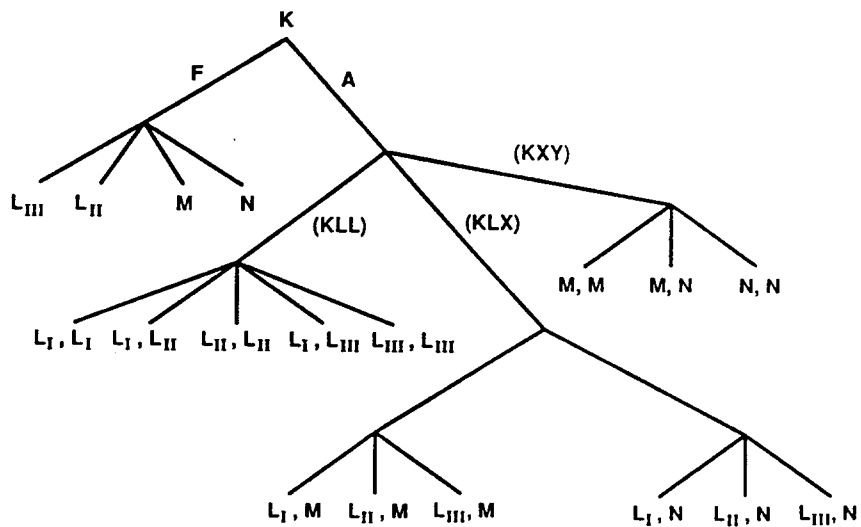
Fig. 7C. Partial relaxation cascades from the K shell.

PAIR SECONDARY PRODUCTION
# PROBABILITY DISTRIBUTION FUNCTION
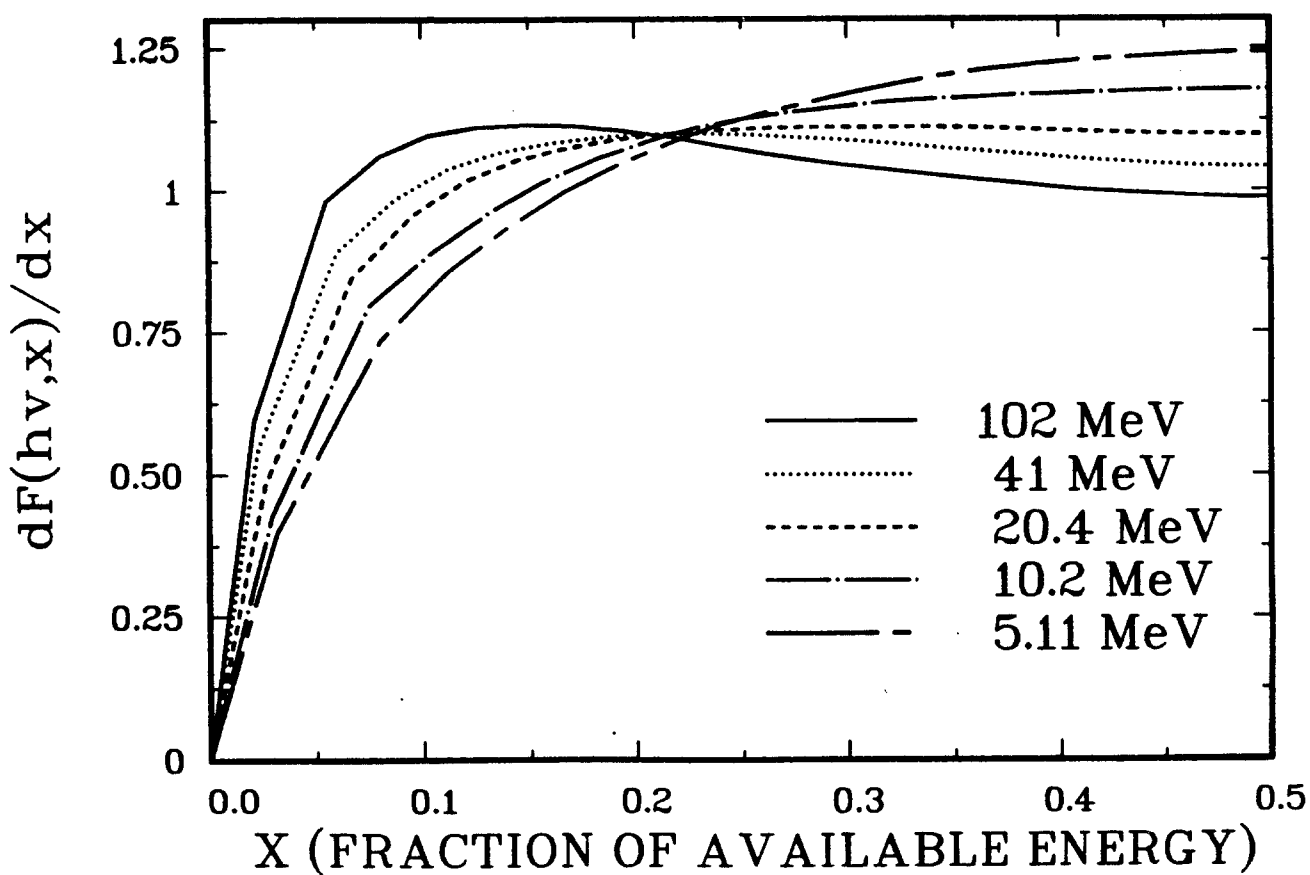
Fig. 8. Pair secondary production probability distribution functions vs. the fraction of available energy.

APPENDIX A.   CODE INDEX

EQUATION	ROUTINES	VARIABLES
I.24	EFABCK, RITE	–
II.3	XEEMOL	–
II.5	XEPMOL	–
II.9	MOL	XTOTCC
II.10	MOL	PRIM
II.15	XESMOL	–
II.18	MOL	SECD
II.23	MOLLER	CSDA
II.25	MOLLER	CSDA
II.30	MOL, MOLLER	ASLT, RESTR
II.31	PREPD	–
II.32	MOL, MOLLER	ALST1, RESTR1
II.33	MOL, MOLLER	ALST2, RESTR2
II.36	STERN	DENMAT
III.1	XBD	–
III.8	E2EBRM	XTOTCC
III.9	E2EBRM	BXSEE
III.17	E2PBRM	BXSEP
III.18	BCOF	–
III.21	E2EBRM	BXSEE

III.23	E2EBRM	BXSEE
III.28	E2EBRM	BSLT, RESTR
III.31	E2EBRM	BSLT1, RESTR1 BSLT2, RESTR2
IV.10	XEAMOT	G
IV.12	GINTP	G
IV.18	BETA	WGXS
V.1	XRAY	–
V.2	XRAY2	–
VIII.3	SIGKN	–
VIII.4	SIGLEG	XSN
VIII.10	SIGKNE	–
VIII.11	SIGLEG	XSN
IX.6	PEELEC	–
IX.10	PHOTOPE	PPXS
IX.11	PEELEC	–
IX.12	FISCHER	–
IX.13	SAUTER	–

Distribution:
Unlimited Release

Air Force Space Technology Center/CA
Attn: J. F. Janni
Kirtland Air Force Base
Albuquerque, NM 87117-6008

Arcon Corp.
Attn: S. Woolf
260 Bear Hill Rd.
Waltham, MA. 02154

Defense Nuclear Agency (5)
DNA/RAEE
Attn: G. Davis
       M. Owais
       B. Prasad
       S. Rosenbloom
       R. C. Webb
Washington, D.C. 20305

Electromagetics Applications
Attn: J. Elliott
P. O. Box 260263
Denver, Co. 80026

Grumman Aerospace Corporation
Attn: P. Suh, MS A01-26
Bethpage, N.Y. 11714

JAYCOR (6)
Attn: J. Kennedy
       B. Passenheim
       B. Seidler
       D. Walters
       J. Wondra
       A. Woods
P. O. Box 85154
San Diego, CA 92138

JAYCOR
Attn: E. Wenaas
1608 Spring Hill Rd.
Vienna, VA. 22182

KTECH Corp. (2)
Attn: A. J. Smith
       E. B. Mann
901 Pennsylvania N.E.
Albuquerque, N. M. 87110

Kaman Sciences (2)
Attn: D. Muth
       T. Stringer
P. O. Box 7463
Colorado Springs, Co. 80933

Lawrence Livermore National Laboratory (5)
Attn: D. Nielsen, L95
       L. Margolin, L18
       P. Soran, L16
       J. Rathkopf, L-298
       D. L. Shaeffer, L-228
P. O. Box 808
Livermore, CA 94550

Los Alamos National Laboratory (14)
Attn: B. A. Clark, MS-B226
       H. Hsu, MS-D410
       B. Kelleher, MS-F611
       J. Mack, MS-E554
       J. E. Morel, MS-B226 (10)
P. O. Box 1663
Los Alamos, NM 87544

Mission Research Corp.
Attn: D. P. Snowden
5434 Ruffin Rd.
San Diego, CA. 92123

National Energy Software Center
Argonne National Laboratory
9700 South Cass Avenue
Argonne, Illinois 60439

Radiation Shielding Information Center, RSIC (10)
Oak Ridge National Laboratory
Oak Ridge, TN 37831-6362

Rome Air Development Center
Attn: J. C. Garth
Hanscom AFB, MA 01731

Science Applications Int'l Corp.
Attn: J. Gates
2860 S. Circle Dr. / Suite 2340
Colorado Springs, Co. 80906

Science Applications Int'l Corp.
Attn: D. Frederick
21151 Western Ave.
Torrance, CA 90501

Science Applications Int'l Corp.
Attn: R. Weitz
2109 Air Park Rd. SE
Albuquerque, NM 87111

Science Applications Int'l Corp. (3)
Attn: K. Adams
      W. L. Chadsey
      J. Tigner
1710 Goodridge Dr.
McLean, VA. 22102

University of Arizona
Attn: W. L. Fillipone
Dept. of Nucl. Eng.
Tucson, AZ 85721

University of New Mexico (2)
Dept. of Nucl. Eng.
Attn: M. Lazo
      A. Prinja
Albuquerque, NM 87131

Weapons Laboratory
Attn: G. Radke, WL/NTCSS
Kirtland Air Force Base
Albuquerque, NM 87117

WJSA
Attn: E. Alcaraz
1901 North Ft. Meyer Dr.
Suite 803
Arlington, VA 22209

Atomic Weapons Establishment, N54
Attn: A. C. Douglas
Aldermaston, Reading RG7 4PR
ENGLAND

Osaka Prefectural Radiation Research Institute
Attn: T. Tabata
Sakai, Osaka 593
JAPAN

1200 J. P. VanDevender
1220 D. Anderson (2)
1230 J. E. Powell
1231 J. R. Lee
1231 L. J. Lorence (35)
1231 J. A. Halblieb
1231 R. P. Kensek
1231 T. W. L. Sanford
1231 V. Harper-Slaboszewicz

1231 G. Valdez (5)
1232 W. Beezhold
1232 W. P. Ballard
1232 D. E. Beutler
1232 R. E. Craven
1233 L. M. Choate
1233 M. A. Hedemann
1234 G. T. Baldwin
1234 D. L. Fehl
1237 L. P. Mix
1262 T. A. Mehlhorn
1262 W. E. Nelson
1265 M. A. Sweeney
2320 J. H. Renken
2321 E. F. Hartman
2321 D. C. Iwan
2322 G. J. Scrivner
2322 A. Badruzzaman
2322 C. Drumm
2322 W. C. Fan
2322 T. A. Haill
2322 C. N. Vittitoe
7542 V. I. Bateman
9112 S. A. Dupree
9249 T. P. Wright